Fall 2011

Design of a current probe for measuring ball-grid-array packaged devices

Tianqi Li

Department:

DESIGN OF A CURRENT PROBE FOR MEASURING BALL-GRID-ARRAY PACKAGED DEVICES

by

TIANQI LI

A THESIS

Presented to the Faculty of the Graduate School of the

MISSOURI UNIVERSITY OF SCIENCE AND TECHNOLOGY

In Partial Fulfillment of the Requirements for the Degree

MASTER OF SCIENCE IN ELECTRICAL ENGINEERING

2011

Approved by

Dr. David J. Pommerenke, Advisor
Dr. Jun Fan
Dr. Daryl G. Beetner

ABSTRACT

A current probe to measure BGA ball currents via magnetic induction has been designed. The probe is manufactured on a 4 layer flex circuit and has been validated by full wave simulations and measurements. The feature size of the probe is very tiny that it almost pushes the limit of flex-circuit technology. Several critical manufacturing problems were happened, and they have been solved now. The probe allows measuring currents of a 1 mm pitch BGA ball directly. Its operating frequency stretched from tens of MHz up to 3GHz. The BGA probe's mutual inductance is approximately11 pH, and with amplifiers the signal is large enough to be visible in real time on an oscilloscope. Moreover, a frequency-domain-calibration program has been developed to correct the measured data. And a FPGA DUT board is designed and manufactured, to demonstrate the application of the BGA probe. ADS model is also developed to show the principle of how the probe works.

ACKNOWLEDGMENTS

I would like to express my sincere gratitude to Dr. David Pommerenke, my advisor, for his advice, instructions, and encouragement on my research work, financial support to my study and direction for this thesis during my pursuit of the Master's degree. I have learned countless things from him about the academic aspect of my research including all the theoretical and experimental knowledge and the skill for writing and presentation.

I would like to thank Dr. Jun Fan, for his excellent teaching, which helped me a lot to understand electromagnetics and build a solid knowledge basis for my research.

I would like to specially thank Dr. Daryl Beetner and Dr. James Drewniak for their valuable advice and support on my research projects and thesis.

I would like to thank Ji Zhang, for his preceding work of my thesis project. His efforts helped to build a good basis for my thesis work.

I would also like to thank all other faculty members in EMC lab for teaching me in the classes and providing me with a great research environment. I would like to express my appreciation to all the students in the EMC lab for their teamwork. I am proud that I was a member of such an exceptional lab in EMC area.

Lastly, I am deeply grateful to my family and parents for their constant support and encouragement.

TABLE OF CONTENTS

LIST OF ILLUSTRATIONS

LIST OF TABLES

1. INTRODUCTION

1.1. PROJECT MOTIVATION AND OBJECTIVE

For power integrity, signal integrity and EMC analysis of high speed ICs, there is a need to measure currents at specific power pins of the ICs, especially, if many pins are connected in the same net, and it is of interest how the current is shared. Considering a case of designing power distribution network (or PDN) on a PCB, voltage and current variations are major concerns of interest when studying the synchronized switching noise (or SSN) within the PDN. The dynamic current is less studied as compared to voltage because it is difficult to measure the dynamic current over a wide frequency range [1].

As technology advances, more ICs and devices are adopting BGA packages in order to reduce product size. This makes current measurements even harder, because the IC balls and their traces, which buried underneath the package body, are hard to be accessed by direct-probing. At present, there is no solution to solve such a problem. Though some works were done to measure currents of specific networks by integrating current sensors into the device-under-test (or DUT) [2], they are not general-purpose-solutions because it is unachievable or too costly to integrate current sensors for every pin in a large-scale-IC. Due to similar reasons, it is not applicable to embed many probes into a PCB to measure every pin of an IC under interest. In this situation, an objective is proposed to design a probe that can measure the current of a specific ball on a BGA package, as well as providing the flexibility for users to change measurement locations.

Several possible current measurement methods, that could be used to achieve the objective, are discussed in chapter 1.2. And the physics of the current sensor that used in this project is illustrated in chapter 2.1. In chapter 2.2, the details of implementing the BGA probe are depicted.

Chapter 3 is devoted for the characteristics of the fabricated probe, both in frequency domain and time domain. The frequency domain characteristics are validated through full-wave simulations and circuit simulations. A frequency domain calibration is performed to correct the time domain measurement results. Such a calibration process has been validated through time domain calibration.

Finally, in chapter 4, a demonstration is provided for showing an application of such a BGA current probe to measure the current waveform of a Vdd core power pin on a BGA-packaged FPGA device. And especially, a method of using BGA-socket-adapter system is introduced, to eliminate the cumbersome BGA re-soldering job if users want to use just one probe to measure different balls.

1.2. METHODOLOGIES

Following major factors, such as size, load effect, bandwidth, complexity and shielding effectiveness, should be considered, when choosing suitable method that can be adopted as the underlying physics of the BGA probe.

Shunts are the most cost effective method [3]. By inserting a small resistor into the circuit-under-test, the current flow through the circuit could be obtained by measuring the voltage across the shunt resistor and divided by the resistance value.

One problem of the method is that the shunt actually affects the circuit-under-test, or the load effect cannot be negligible. To solve this problem, some isolation techniques were introduced in [4] [5] [6], while this increases the cost and complexity.

Another problem is that the circuit designer has to firstly place a 0Ω resistor into the circuit-under-test in order to replace it with a shunt resistor later for measure the current, and such a resistor has to be accessible for probing. This is usually unachievable in the high-density-routing-area where the BGA device-under-test locates.

The measurement of currents can in principle be achieved by using a loop probe, such as a Rogowski coil [8], to measure the induced magnetic field of the current source. The method reduces load effect since there’s no galvanic connection between the probe and DUT.

Limitation of using loop probes is that DC cannot be measured, because DC cannot generate any field variation that can leads to field-induction to the loop probe.

An example of using a loop probe to measure the current of a ball is illustrated in Figure 1.1. The magnetic field wraps around the ball penetrates the loop area and cause induced voltage across two ends of loop. The current that induced from the magnetic field can be calculated by measuring the voltage drop across a known load resistance.

The sensitivity of such a probe is low since there is only one turn of the loop, and the space between two balls is very limited.

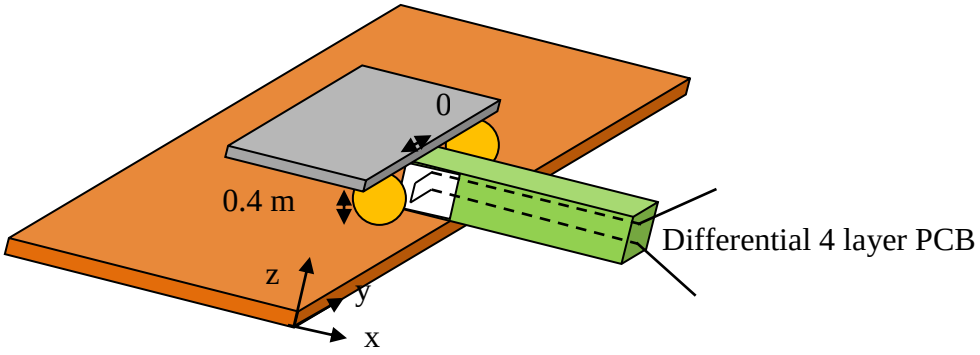

Figure 1.1. A Possible Loop Probe Design

The method showed in Figure 1.1 would have very limited sensitivity, because the loop area is so small due to the very limited region between two balls on a BGA package, and there's only one turn in this design.

In Figure 1.1, the loop probe could be changed to probes based-on Giant Magnetoresistive [9] or Giant Magneto Impedance [10] sensors, in order to obtain higher magnetic field sensitivity. But the problem is that it is hard to shield the sensor in order to avoid magnetic coupling from adjacent balls. Due to the same reason, it is difficult to design a Magnetic-Optical based probe [11] and insert it underneath a BGA package to measure current of a specific ball, though MO based probe does not disturb the filed-under-test and can be built very small.

After evaluating the trade-off among the factors, such as size, sensitivity, shielding and complexity, PCB-based Rogowski coil is an acceptable option. The reason will be discussed in chapter 2.

2. PHYSICS AND IMPLEMENTATION OF THE ROGOWSKI-COIL-BASED BGA CURRENT PROBE

2.1. PHYSICS OF THE ROGOWSKI-COIL BASED BGA CURRENT PROBE

2.1.1. The Magnetic Field Distribution around a Ball. The BGA current is measured through magnetic field induction. For simplicity, magnetic field in this thesis will be called H-field, and electric field will be called E-field. The H-field generated by the current going through balls of BGA package can correctly represent the magnitude of the current. Voltage variation of the ball-under-test may cause electric field, or E-field, coupling, which should be shielded or suppressed as much as possible when designing an H-field probe. Figure 2.1 shows distribution of magnetic field surrounding a ball when a minus z-direction current is defined. Thus, a well-designed H-field probe could be used to measure the current through one ball, in the frequency range from MHz up to GHz.

In reality, at high frequencies the current does not flow through the ball, but flow on the surface of the ball. But this does not matter for the Rogowski coil.

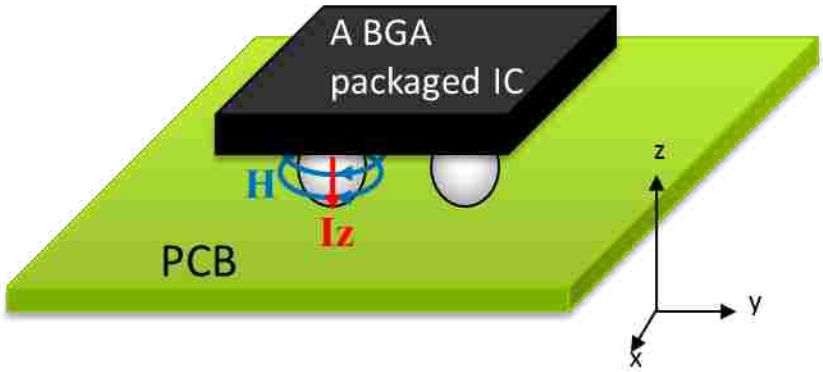

Figure 2.1. Current and H-field Distribution around the Balls of BGA package

2.1.2. Rogowski Coil Structure. The current probe's structure is based on the Rogowski coil. A Rogowski coil wraps around the magnetic field of a current [7]. The magnetic field is used for current measurement through induction, thus, this design can

be used for measuring AC currents, but no DC current. A general principle of such a Rogowski coil is shown in Figure 2.2.

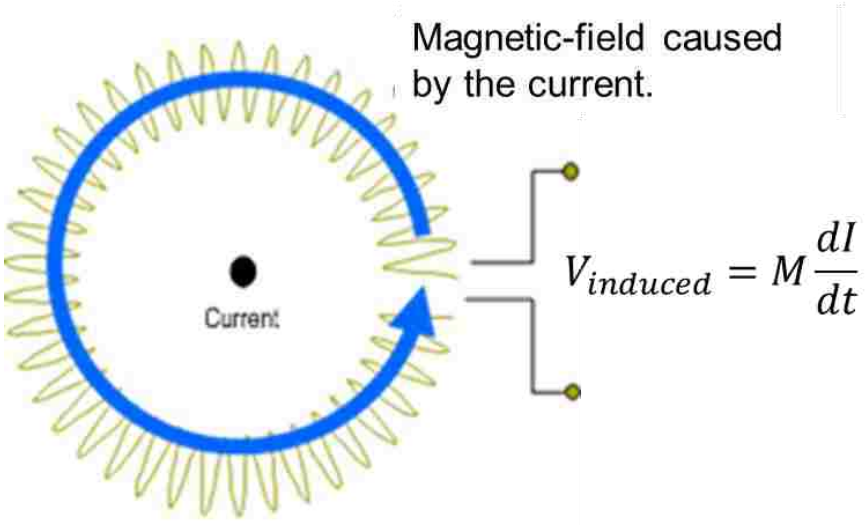

Figure 2.2. Rogowski Coil Sensor

Then current-under-test can be obtained by measuring the voltage across the two ends of the coil. One thing needs to be mentioned that the measured voltage does not equal to the induced voltage, because in practical case, there is usually a 50 ohm load impedance, which is actually the input impedance of an instrument, across the two ends of the coil. Thus, if regarding the coil as a source with source impedance that is defined as Z_{coil}, the relationship between measured load-voltage and current-under-test can be described in the following equation:

$$\mathrm{V_{induced}} = M * \frac{dI}{dt} \tag{1}$$

$$\mathrm{V_{load}} = V_{induced} * \frac{50}{50+Z_{coil}} = \mathrm{M} * \frac{\mathrm{dI}}{dt} * \frac{50}{50+Z_{coil}} \tag{2}$$

Where $V_{induced}$ is the induced voltage, M is the mutual inductance between the coil structure and current source, which can be characterized by measurements. The unknown value I is the current-under-test.

In this way, the current I can be calculated by doing integration, as what described in the following equation in time domain.

$$I = \int \frac{V_{load}}{M} * \frac{50+Z_{coil}}{50} * dt \quad (3)$$

In this thesis, such a calculation is actually done in frequency domain, which will be discussed in Chapter 3.3.4.

The Rogowski coil structure could be implemented in a four-layer PCB or flex-circuit, in such a way showed in Figure 2.3. Four shadow areas, which could be penetrated by magnetic flux, are implemented in a series-circuit fashion by the copper traces in 2nd and 3rd layer. The 1st and 4th layer are used for shielding.

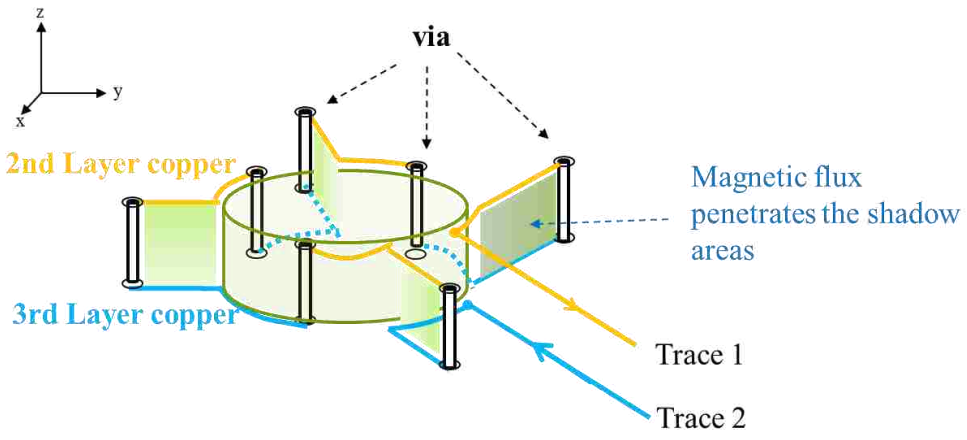

Figure 2.3. 3-D view of the Rogowski coil structure in layered flex-circuit

Such a Rogowski sensor structure can be applied underneath a BGA package to measure current of a specific ball. The principle concept is shown below in Figure 2.4. In this figure, a simplified configuration is shown to illustrate where to place a Rogowski

sensor to measure current of a specific ball. The yellow circles indicate the balls of a BGA package. Red lines define the outline of the current probe. The Rogowski current sensor consisting of four loops, which are shown in blue color, locate at the four corners of the probe. The probe needs to be positioned under a BGA package in such a way that the ball-under-test should go through the center measurement hole of the probe.

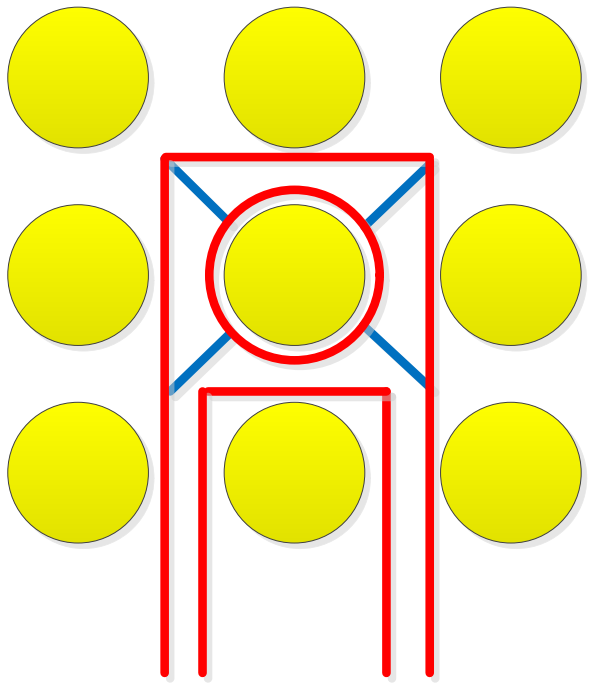

Figure 2.4. Rogowski Structure for Current Measurement of a Ball

2.2. IMPLEMENTATION OF THE BGA CURRENT PROBE

2.2.1. Layout of the BGA Probe. As mentioned above, the PCB layout includes four layers: the top layer and the bottom layer are covered by copper for shielding from E-field coupling. The second layer and the third layer are the main structure for Rogowski coil probe. As shown in Figure 2.5, the layout for this probe includes two portions: the Rogowski coil at tip area and the 50-ohm output trace part.

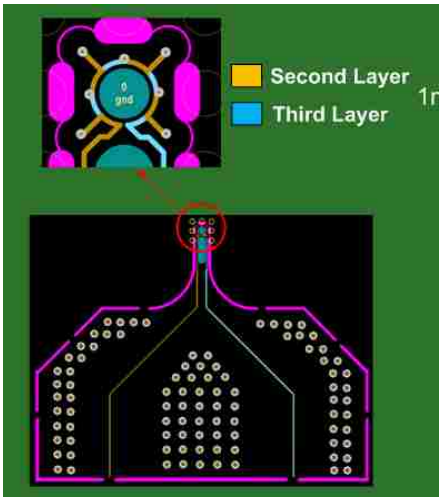

Figure 2.5 Layout of the Rogowski Coil of BGA current probe

At the probe tip region, as shown in the enlarged view in Figure 2.5, there are four coil loops located at the four corner of the pattern in order to accumulate the magnetic flux caused by the current within the coil. For 3-D view of the coil structure, please refer to Figure 2.3.

For the 50 ohm output trace part, at the very end of the traces, two groups of vias route out the signal from internal layers to the top layer, as shown in Figure 2.6.

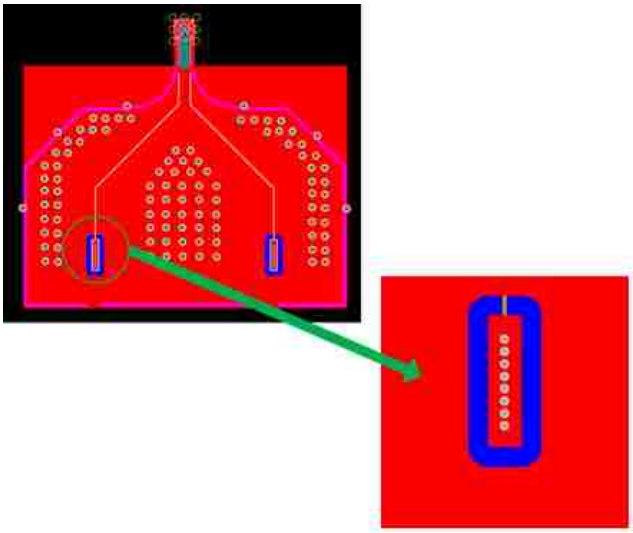

Figure 2.6 Layout of the Output Pad of BGA current probe

2.2.2. Fabrication Technology. A four-layer flex circuit is chosen to achieve the requirements for high precision structure of the BGA current probe, because that when the probe's feature-size goes too small, the probe could be very fragile if fabricated based on PCB technology. Before the flex-circuit version, a PCB version was fabricated but showed problems of over-sensitivity to mechanical vibration, heat change and very low yielding rate because of extremely small feature sizes, such as the blind micro-vias with 2 mil diameter, and 2 mil spacing between the traces and plated edges.

2.2.3. Dimensional Tolerances and Special Fabrication Considerations. The BGA probe is designed to be applied to 1mm BGA package. The 1mm-pitch BGA package is shown in Figure 2.7. The BGA package information is quoted from FPGA devices datasheets from Altera Cooperation.

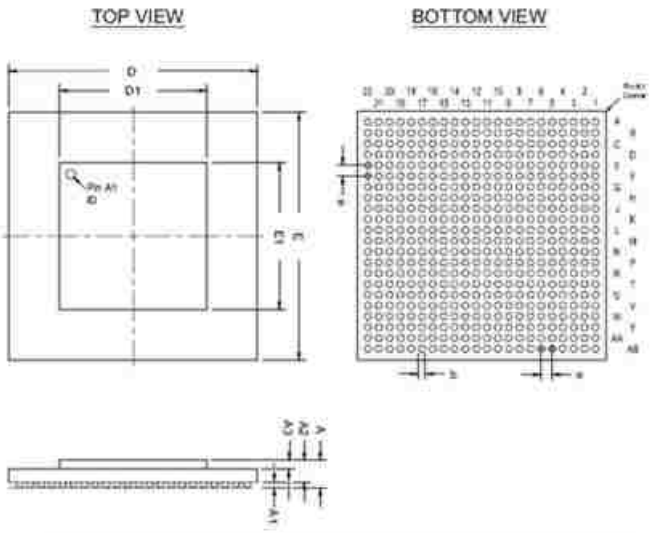

Package Outline Dimension Table			
Symbol	Millimeters		
	Min.	Nom.	Max.
A	2.10	2.30	2.50
A1	0.40	0.50	0.60
A2	1.50	1.80	2.10
A3	0.75	0.85	0.95
D	23.00 BSC		
D1	11.00 (Typ)		
E	23.00 BSC		
E1	9.00 (Typ)		
b	0.50	0.60	0.70
e	1.00 BSC		

Figure 2.7. Dimensional information of a 1mm BGA package [12]

The package drawing shows a 1 mm pitch, and 0.6 mm ball diameter. When designing the layout of the BGA probe, mechanical tolerance and margin should be considered in “worst case”, i.e. the largest ball size of 0.7mm and lowest thickness of 0.4mm for designing. In practical, thickness of the BGA probe cannot exceed 0.3mm, or the BGA packaged device cannot be soldered to PCB firmly due to lower part of balls cannot be buried into soldering tin.

The outline of the probe is shown as purple lines in the Figure 2.8. The outline or edge should be edge-plated in order to avoid unwanted E-field coupling. Moreover, solder mask should be applied outside the plated edge, or the plating may be shorted with adjacent BGA balls.

The thin purple lines in Figure 2.8, around the probe tip area, are strictly defined for its mechanical tolerances. If such an outline is made larger, the probe tip would collide with adjacent balls; if made smaller, clearance between the outline and traces would be too small to be manufactured. Edge-plating and its covered solder mask would even aggravate such an issue.

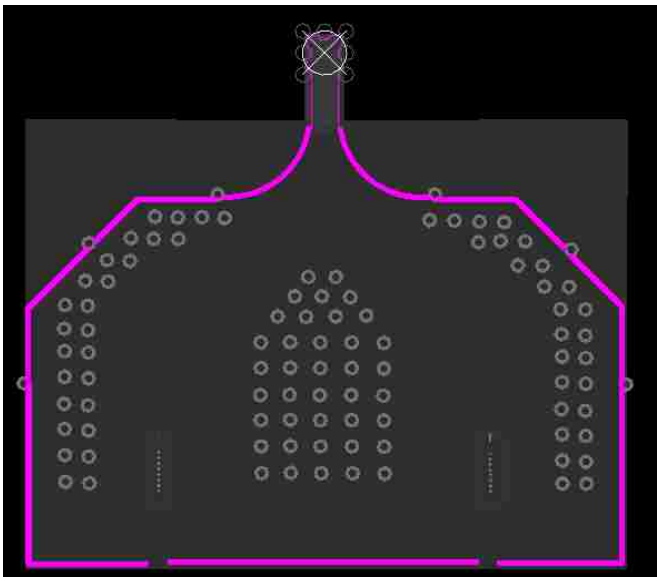

Figure 2.8. Outline of the BGA probe

The enlarged view of the tip area is shown in Figure 2.9.

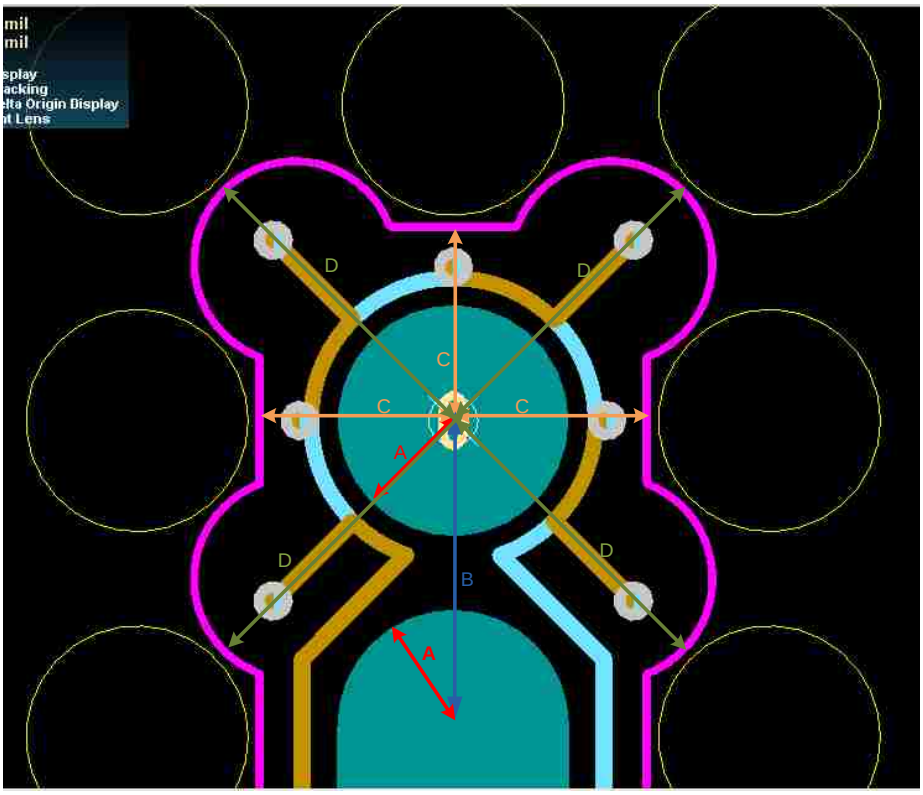

Figure 2.9. Enlarged View of the BGA Probe Tip Area

The purple lines and curves stand for the outline or shape of the probe tip area. The centered big blue round area stands for a hole, which allows the ball-under-measurement could go through. Yellow circles in Figure 2.9 show the supposed positions of adjacent balls of a BGA package. Yellow and light blue lines stand for copper traces in layer 2 and 3, respectively. Seven vias used for connecting layer 2 and 3 traces, shown in grey rings, are with diameter of 2mil. The dimensional tolerances of the probe are defined by means of the distances marked by A, B, C, & D, shown in the Figure 2.9. The tolerances are listed in Table 2.1.

Table 2.1. Dimensional Tolerances of the BGA Probe

Distance	Dimensional Tolerances
A	Radius of the measurement-hole at center. Should be larger than 0.35mm, and this hole is hard to be plated on its internal wall. In gerber file, the actual designed distance is 0.365mm, so margin is 0.015mm, or around 0.6mil.
B	Distance from the hole center to the adjacent hole center locates at upper end of the slot. Should not be greater than 1mm. The actual design is 1.05mm in gerber file, so margin is 0.05mm, or 2mil. Note that the slot should not be plated.
C	Distance from the hole center to straight edges. Should not be greater than 0.615mm, actually designed as 0.648mm, so margin is 1mil.
D	Distance from the hole center to circular edges. Should not be greater than 1.06492mm, actually designed as 1.03097mm**,** so margin is margin 1mil.

2.2.4. Stack-up of the BGA Probe. Total thickness of the probe should be controlled to less than 200 um or the BGA cannot be mounted to PCB firmly because the minimum ball height of FBGA is 400 um. And the distance between layer2 and 3 should be as large as possible to increase the available area for magnetic flux to penetrate, thus maximizing the sensitivity. The contradiction of keeping distance between layer 2 and layer 3 as large while minimize the total thickness, is a major trade-off of designing the probe.

The stack-up of the BGA probe is showed in Figure 2.10. All numbers are in the unit of um. The total thickness of the probe is 183.2 um, and distance between layer 2 and layer 3 is 91 um. Layer 1 and Layer 4 are used for shielding planes.

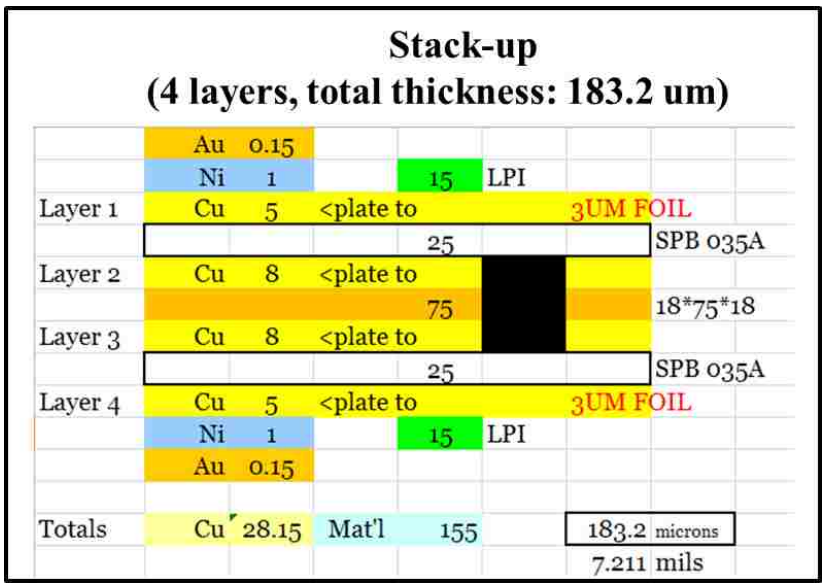

Figure 2.10. Stack-up of the BGA probe

2.2.5. The Fabricated BGA Probe. The fabricated probe is shown in the Figure 2.11. The center hole of at the probe tip region has a diameter of 0.7mm, which allows a ball of 1mm-pitch package to go through.

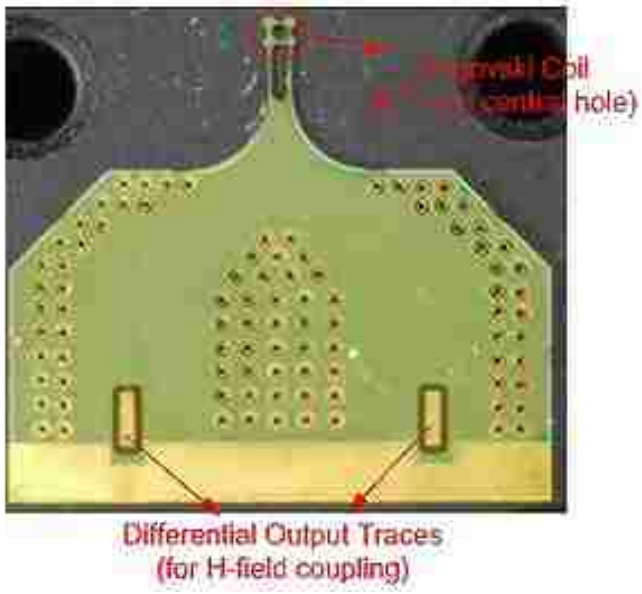

Figure 2.11. The Fabricated BGA Current Probe

As shown in Figure 2.12, the fabricated probe conforms to the structure of a 1mm BGA package quite well.

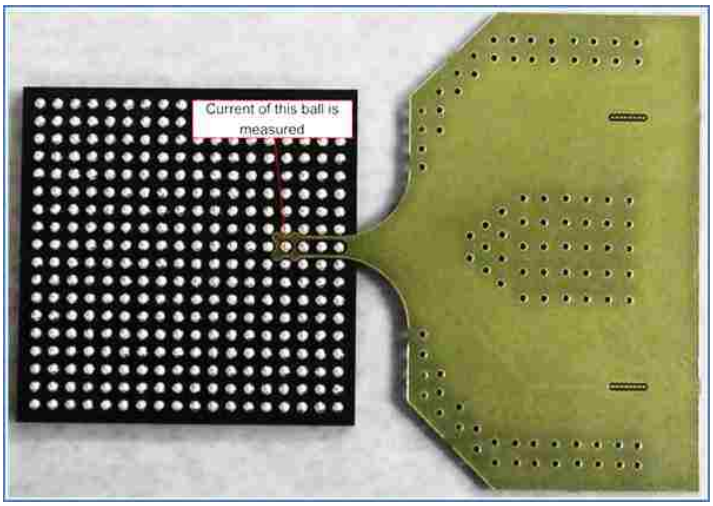

Figure 2.12. The fabricated BGA probe applied to a 1mm BGA package

3. CHARACTERIZATION OF THE BGA CURRENT PROBE

3.1. FREQUENCY DOMAIN CHARACTERIZATION

3.1.1. The BGA Probe Assembly. The schematic of the probe assembly is shown in Figure 3.1. The characterization assembly includes two parts: excitation part and the BGA probe. In the excitation part, an excitation wire with a load resistor goes through the center measurement hole of the probe tip and connects to a SMA connector, which is defined as port 1. The load resistor could be short, open or match, depending on different characterization purposes.

Voltage and current variation in the excitation wire would cause E-field coupling and H-field coupling to the BGA probe, respectively. Consequently, differential mode of the signals on port 2 and port 3 is related to H-field coupling, and common mode is relevant to E-field coupling.

Ideally, E-field coupling won't affect current measurement results since the common mode signal would be decoupled from measurement results by taking the difference between the two output signals on port 2 and 3. While in practical case, due to limited common mode rejection ratio, E-field coupling may actually contribute to the output differential signal. Therefore, E-field coupling should be controlled as least as possible.

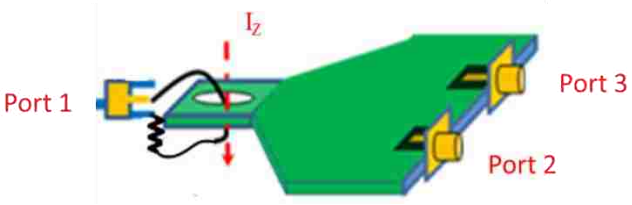

Figure 3.1. Schematic of the test setup to characterize the BGA probe

For frequency domain characterization, S-parameters of the 3-port network are measured. For time domain characterization, a known excitation signal is exerted at port 1 and output waveform will be read at port 2 and 3.

To build a probe assembly, the flex circuit could be mounted on a solid copper board and have its two signals routed out by two highly symmetrical micro-coaxial cables, which are covered by couples of ferrite beads, as shown in Figure 3.2.

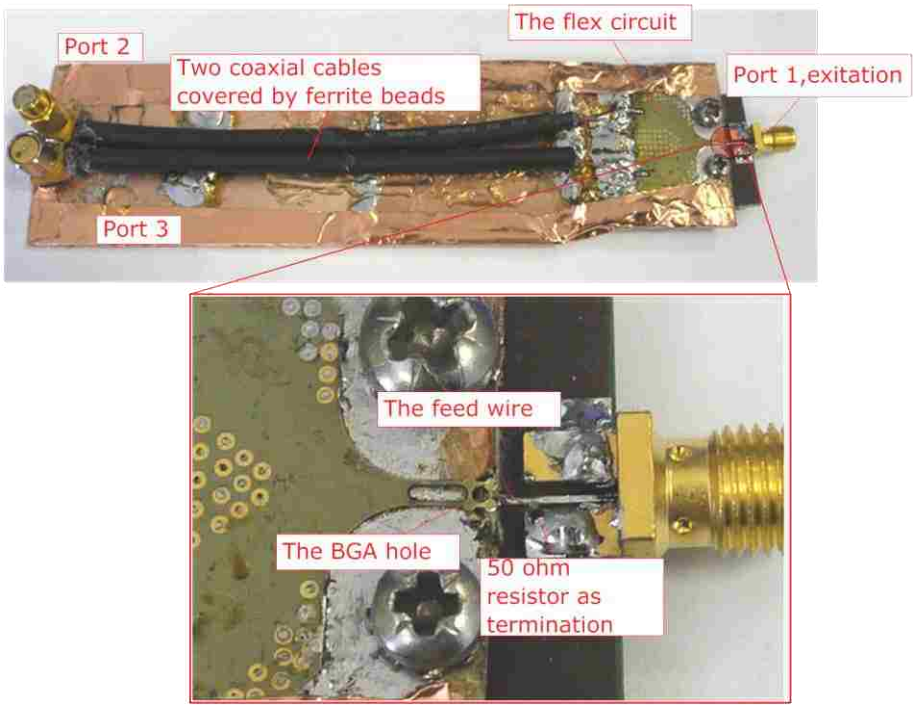

Figure 3.2: The BGA Probe Assembly for Characterization

The two cables route signals out to port 2 and 3. On the other end, a wire, whose current supposed to be measured by the probe, goes through the BGA hole. The wire is stimulated by port 1. Please look at the enlarged picture for details. Note that in Figure 3.2 the wire is 50 ohm terminated while in some measurements it may be changed to open or short conditions.

3.1.2. TDR Response of the BGA Probe Assembly. The probe assembly is verified by TDR measurements. The test setup of TDR measurements is shown in Figure 3.3. One port of the BGA probe connects to the TDR, and the other port is terminated with a 50 ohm load.

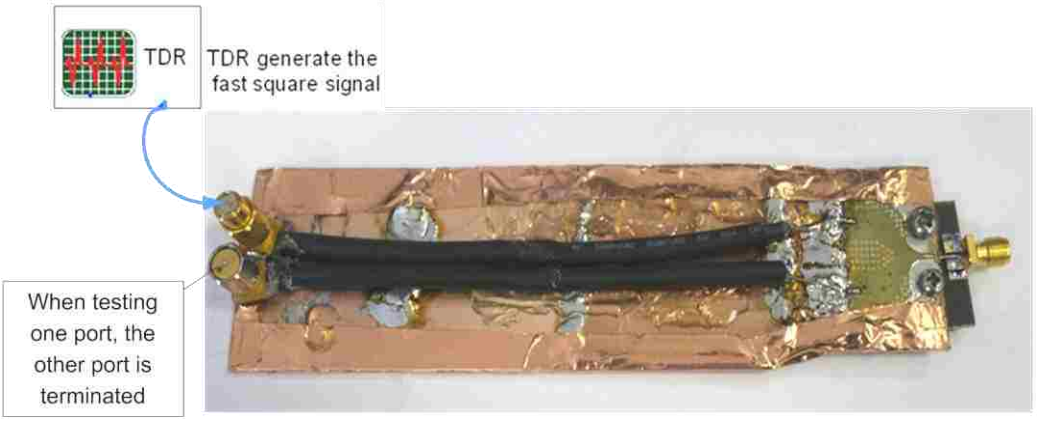

Figure 3.3. Setup for TDR Measurement

The measured TDR response in Figure 3.4 shows that the probe's differential signal channels are basically symmetrical. The difference when looking into port 2 and port 3, is due to an excessive 12.4 fF capacitance located at the junction between coaxial cable and the pad of the BGA probe, of port 3. The self-inductance of Rogowski coil is approximately 700pH. It also could be read that the characteristic impedance of the traces in flex circuit is approximately 40 ohm.

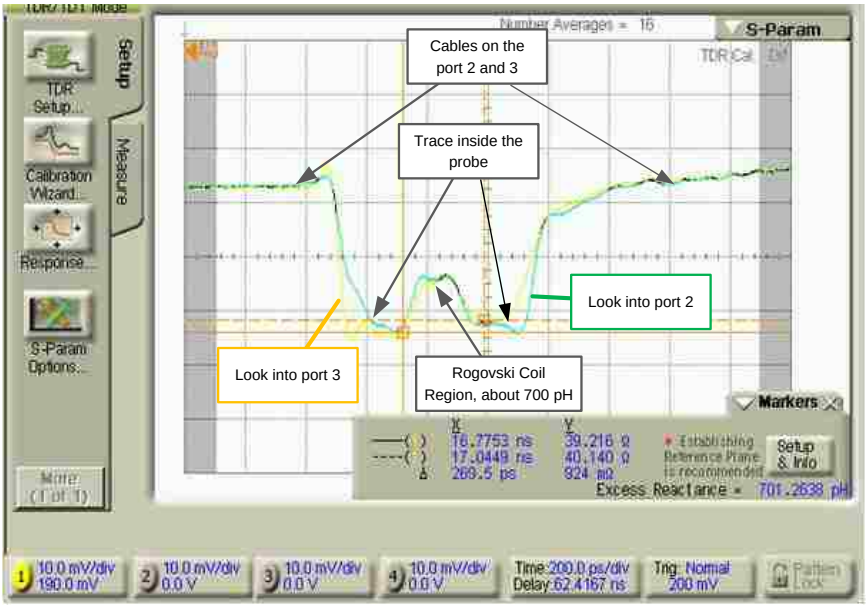

Figure 3.4. TDR Response of the BGA Probe Assembly

The enlarged TDR response of the first falling edge, which is showed in 50ps per division, is illustrated in Figure 3.5. The small amount difference of time indicates the difference in lengths of the differential channels. The difference, which is measured as 8.79ps, stands for a 0.66 mm difference in length between the two signal channels. Such a difference would cause a very small error in measurement results at 3GHz, because the difference would cause approximately 3.8^{o} difference in phase between the two output channels at 3GHz.

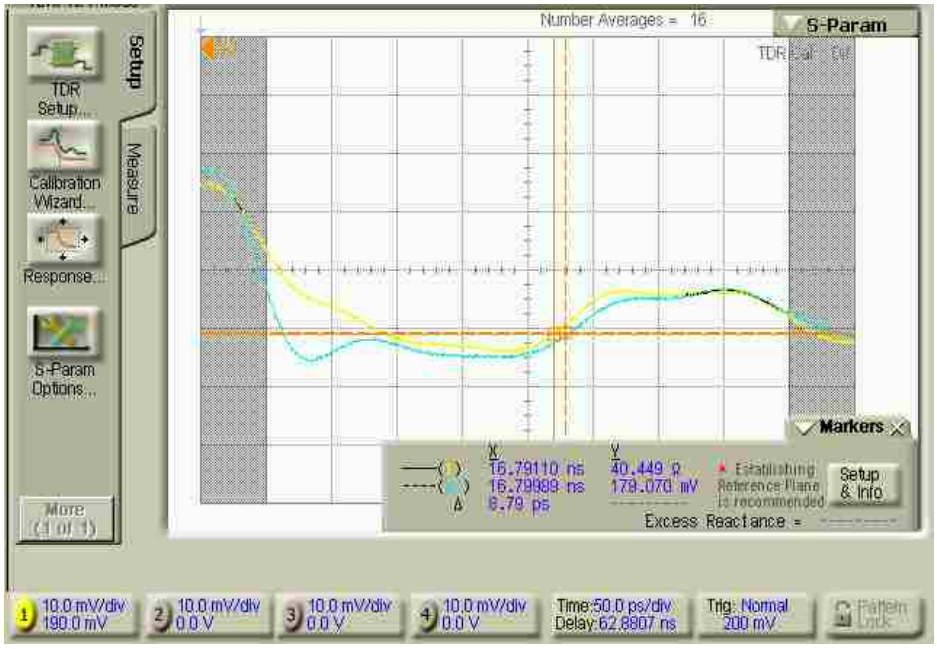

Figure 3.5. Enlarged View of TDR Response of the BGA Probe Assembly

Above figures show that there are very small differences between the TDR responses that exited at port 2 and port 3 respectively. S22 and S33 may be measured to investigate the difference in further.

3.1.3. Test Setup for Frequency Domain Characterization. An example of measuring S31 of the BGA probe assembly is shown in the Figure 3.6. Port 1 is connected to the excitation port of a network analyzer. When measuring port 3, the port 2 need to be matched, and vice versa.

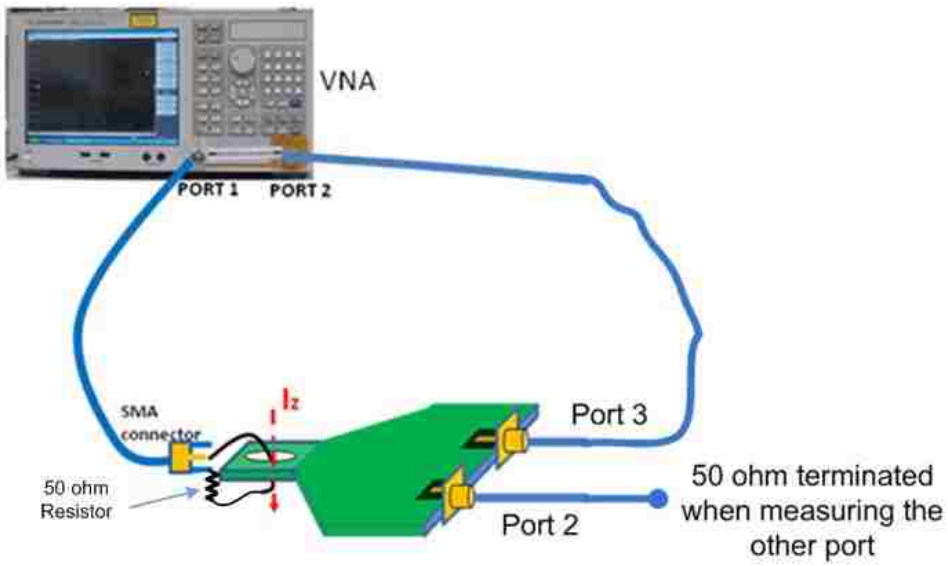

Figure 3.6. Test Setup for Frequency Domain Characterization

As shown in Figure 3.6. Test Setup for Frequency Domain Characterization, a thin wire connected the inner conductor and the outer conductor of the SMA connector expended from PORT 1 of VNA, through a 50 Ohm load resistor. Thus, this wire leads the current going through the hole of the BGA probe.

Since the signal coupled by H-field is in a form of differential signal, i.e., signals on port 2 and 3 should be out of phase. Therefore it could be expected that measured S_{21} and S_{31} should show similar magnitudes but out of phase, if H-field coupling dominates. If E-field coupling exists, there will be magnitude difference between S21 and S31.

3.1.4. Reflection Parameters. The test setup is verified by measuring reflection parameters, i.e. S11, S22 and S33. The S11 should be small because the short wire loop is 50 ohm terminated. In this case the measured results showed in Figure 3.7 are acceptable, which means the wire loop structure is OK.

S22 and S33 is relatively high because that the impedance inside the flex circuit is not 50 ohm, due to the manufacturing limitation. But this is not a critical problem in this case. The similarity of S22 and S33 indicates that the two differential signal channels are basically symmetrical, which conforms to the TDR measurement results.

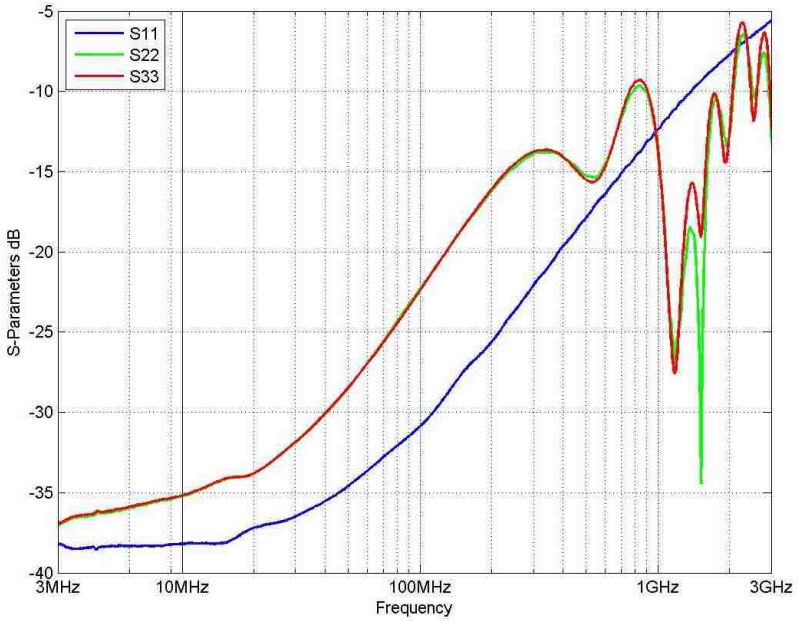

Figure 3.7. Measured S11, S22 and S33 of the BGA Probe Assembly

3.1.5. S-Parameters under Short Condition. The H-field excitation is strongest and E-field coupling is the weakest when DUT wire is short terminated, because the current flowing through the DUT wire is maximized under such condition and voltage minimized. It is necessary to inspect how well the probe can sense magnetic field in this case.

As what can expect, if the probe is H-field coupling dominated, the magnitudes of S21 and S31 should be same and their phases should have a 180^{o} difference. In this case, E-field coupling is minimized. If define the voltage caused by magnetic induction as V_H, and voltage at port 1 is V_1, then there's the relationship:

$$S_{21} = \frac{V_H}{V_1} \tag{4}$$

$$S_{31} = -S_{21} = -\frac{V_H}{V_1} \tag{5}$$

Where V_1 stands for the voltage on port 1, and V_H represents the voltage, which is caused by H-filed coupling, on port 2 and port 3.

Moreover, S21 or S31 should increase as frequency goes up with a 20 dB/decade slope, if S21 is plotted in log-frequency scale, because S21 can be described by the following equation. The equation shows that when the frequency increases by 10 times, the S21 would increase by 20dB.

$$S21(dB) = 20 * \log_{10}\left(\frac{V_H}{V_1}\right) \approx 20 * \log_{10}\left(\frac{j*2*\pi*f*M}{Z_1}\right) \quad (6)$$

Where Z_1 stands for the input impedance of port 1, and M represents the mutual inductance between excitation wire and the Rogowski coil structure at the BGA probe tip region.

The measured results, showed in Figure 3.8 and Figure 3.9, agrees with such an expectation. In the region from 10MHz to 1.5GHz, S21 and S31 basically follow the 20dB/decade slope. In this region, current could be calculated by doing integration of the $V_{measured}$ after offset correction.

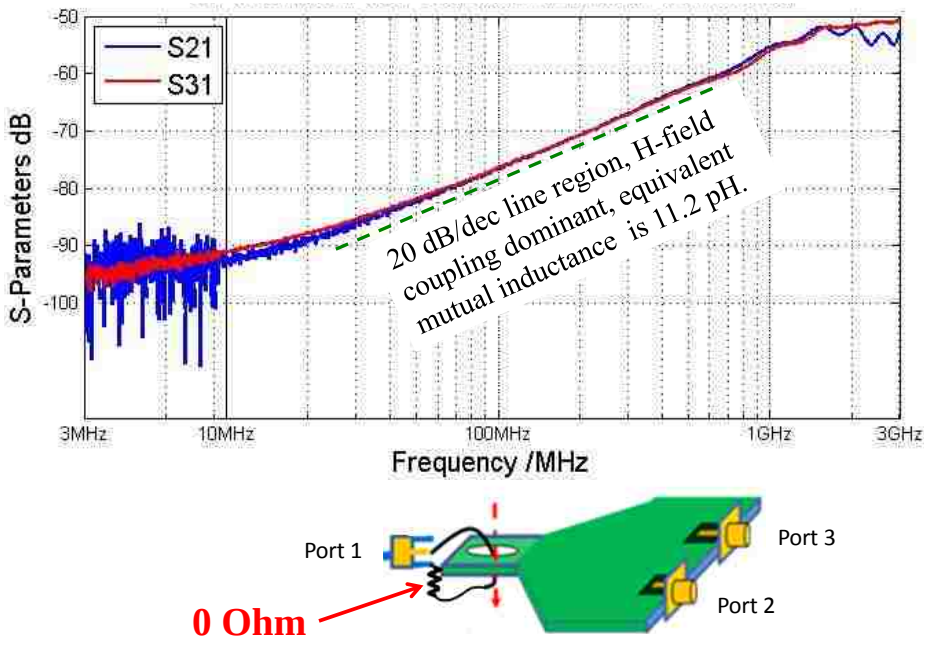

Figure 3.8. Magnitudes of S21 and S31 Measured under Short Condition

The value of mutual inductance between Rogowski coil and the excitation wire could also be calculated by recasting the equation (6). After calculation the value of the mutual inductance is 11.2pH.

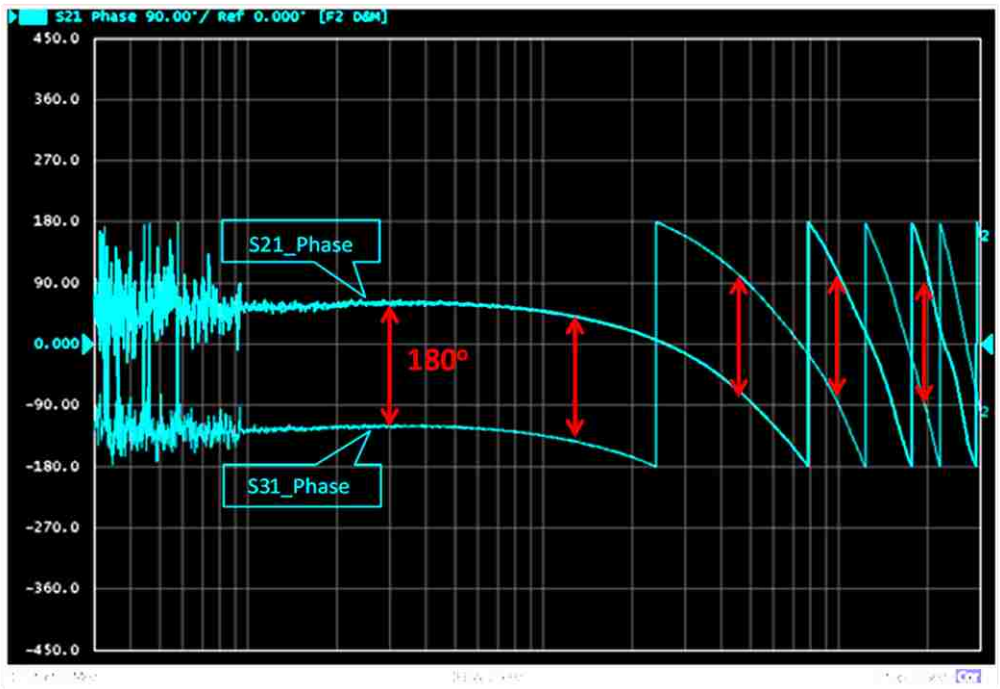

Figure 3.9. Phases of S21 and S31 Measured under Short Condition

S21 and S31 under short condition also indicate that the equivalent mutual inductance of the BGA probe equals to 11.2 pH. The process of calculating the mutual inductance will be explained in Chapter 3.1.9.

3.1.6. S-Parameters under Open Condition. On the contrary, the E-field excitation is maximized and H-field is minimized when the DUT wire is open-terminated, because the current flowing through the DUT wire is minimized. It could be understood of how easily the probe can sense electric field in this case.

As what can expect, if the probe is E-field coupling dominated, both magnitudes and phases of S21 and S31 should be same. If define the voltage caused by E-field

coupling as V_E, and voltage at port 1 is V_1, then the relationship could be described by the following equation:

$$S_{21} = S_{31} = \frac{V_E}{V_1} \tag{7}$$

V_E stands for the E-field induced voltage on port 2 and 3. The measured results, showed in Figure 3.10 and Figure 3.11, agreed with the expectation.

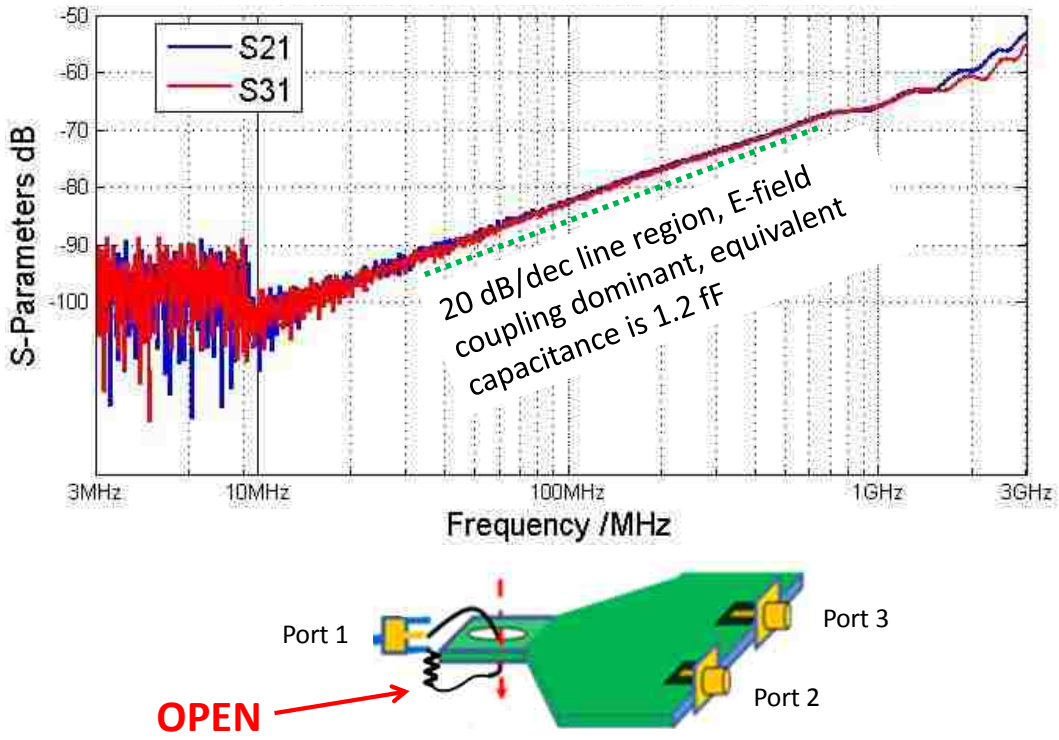

Figure 3.10. Magnitudes of S21 and S31 Measured under Open Condition

Phases of S21 and S31, under E-field coupling dominant condition, are shown in the Figure 3.11. As what can be expected, the S21 and S31 are in phase. And therefore the E-field coupling would contribute common mode of the output signal.

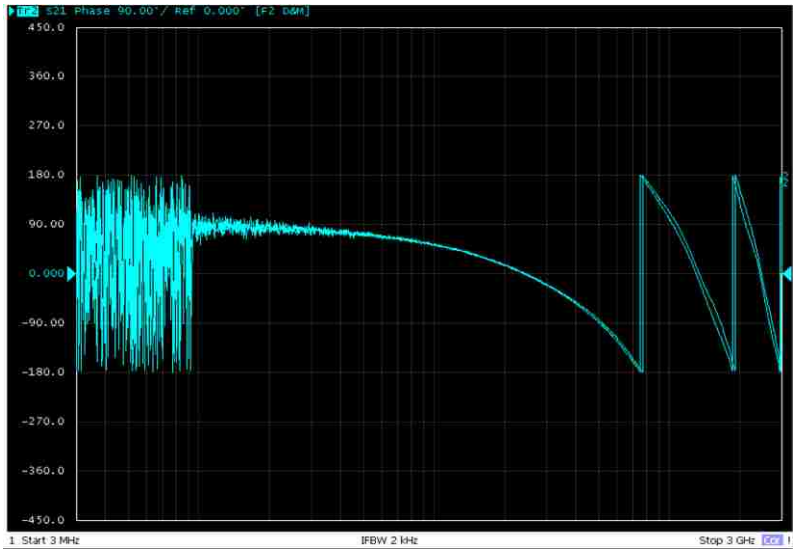

Figure 3.11. Phases of S21 and S31 Measured under Open Condition

By comparing Figure 3.8 and Figure 3.10, it shows that E-field coupling can be as strong as H-field coupling. Then the probe is measured under 50Ω case, in which both H-field and E-field coupling may take effect.

3.1.7. S-Parameters under 50 Ω Matched-Load Condition. In this case, if the degree of E-field excitation is comparable with H-field excitation, or both E and H-field coupling dominates, magnitudes of S21 and S31should be different, because H-field components of port 2 and port 3 are out of phase. Or the relationship could be described as:

$$S_{21} = \frac{V_E + V_H}{V_1} \tag{8}$$

$$S_{31} = \frac{V_E - V_H}{V_1} \tag{9}$$

The coupling can be easier recognized by looking at phase plot. In the frequency range that phases difference between S21 and S31closed to 180 degrees, H-field coupling is stronger and similarly, in the frequency range of that the phase difference closed to 0 degree, E-field coupling dominates.

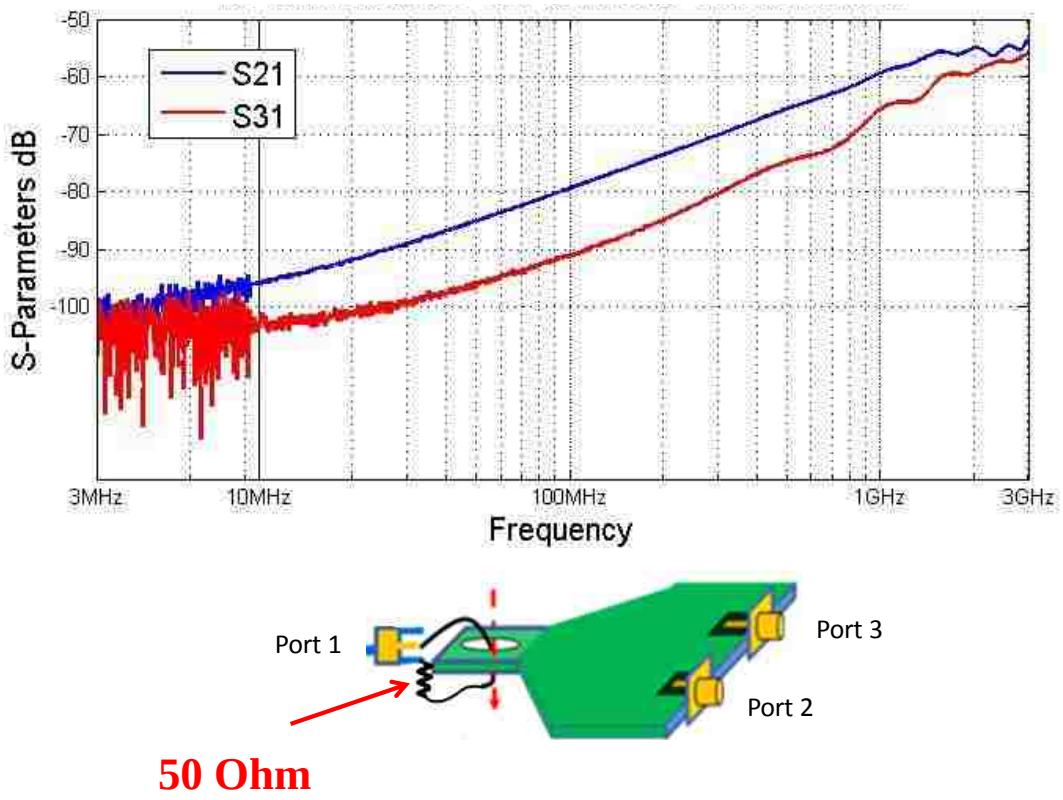

Figure 3.12. Magnitudes of S21 and S31 Measured under Matched Condition

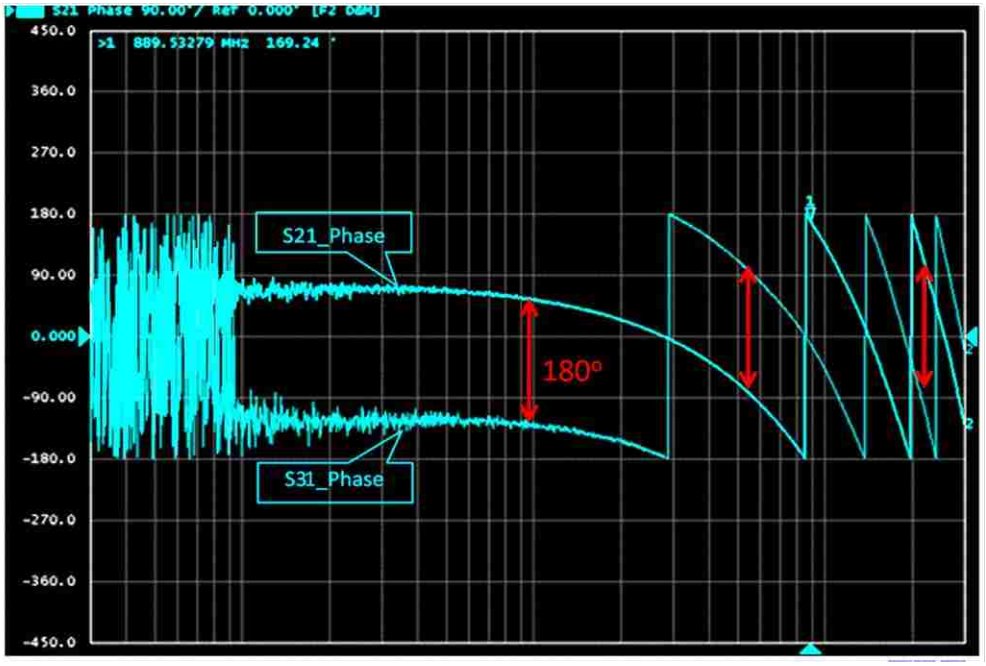

Figure 3.13. Phases of S21 and S31 Measured under Matched Condition

The measured S21 and S31 in Figure 3.12 and Figure 3.13 show different magnitudes, which conform to the expectation. The measured phases indicate that H-field coupling is stronger than E-field coupling because phase difference is closed to180^{o}. To investigate the H-field and E-field coupling strength analytically, the above equations can be recast as:

$$\mathrm{V_H} = \frac{V_1(S_{21}-S_{31})}{2} \tag{10}$$

$$\mathrm{V_E} = \frac{V_1(S_{21}+S_{31})}{2} \tag{11}$$

In this way, the comparison between H-field coupling strength and E-field coupling strength under 50Ω could be calculated, as shown in Figure 3.14. Note: the simulated result showed in the Figure 3.14 is obtained from CST full wave simulation, which will be explained in Chapter 3.2.

The difference between strengths of H-field coupling and E-field coupling can be interpreted as the common mode rejection ratio. The higher the ratio is, the probe is more

insensitive to E-field coupling, i.e. the better on shielding performance. In Figure 3.14, V_H stands for the probe's output voltage signal in terms of H-field coupling or differential output, and V_E represents the probe's output voltage signal in terms of E-field coupling or common mode output. From the Figure 3.14, the common-mode-rejection-ratio could be read as greater than 4 dB below 1.5GHz, under 50 ohm load condition. Under short condition, the rejection ratio would be much higher since E-field coupling is minimized in that case. Therefore, the BGA current probe would generate better result when measuring balls with low impedance.

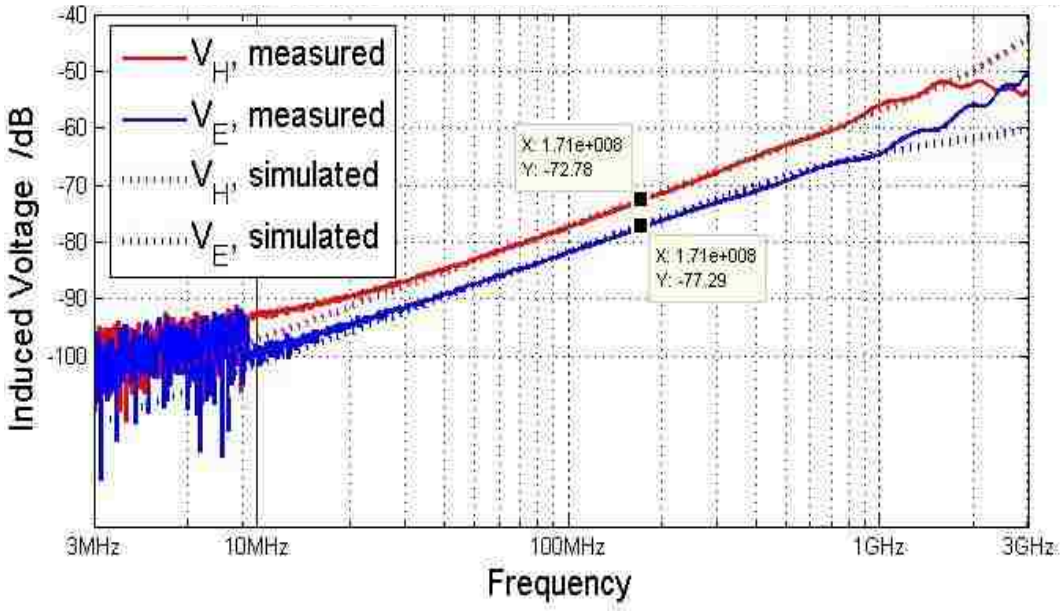

Figure 3.14. H-field Coupling vs. E-field Coupling under 50Ω Load Condition

It is showed that the H-to-E rejection ratio is approximately 4.5dB under matched load condition, which is not a large number. But the impedance of power pin is usually very low, which is similar to the short load condition, in which case the H-to-E rejection ratio could be much higher than that under 50Ω load condition.

Above 1 GHz, the measured result shows non-ideal properties, which are due to the hand-made non-ideal test setup, especially the wire loop shape and size. In reality when the probe applies to real BGA package, the frequency response at high frequency

can be much better or more close to simulation results, because the ball is a relatively more ideal source due to its symmetrical shape.

3.1.8. Shielding Effectiveness of the BGA Probe. The BGA probe should only sense the H-field caused by the current inside the hole. So the parameter of shielding effectiveness should be evaluated to characterize of how well the probe is insensitive to E-field sources and adjacent H-field sources.

The interference from unwanted sources may come from the voltage variations of the ball-under-test, the current and voltage variations of adjacent balls and the ground voltage fluctuations between the probe and device-under-test.

By placing the excitation wire inside and outside the center hole of BGA probe, and comparing their S21, the shielding effectiveness for the fields from the outside could be evaluated, as shown in Figure 3.15.

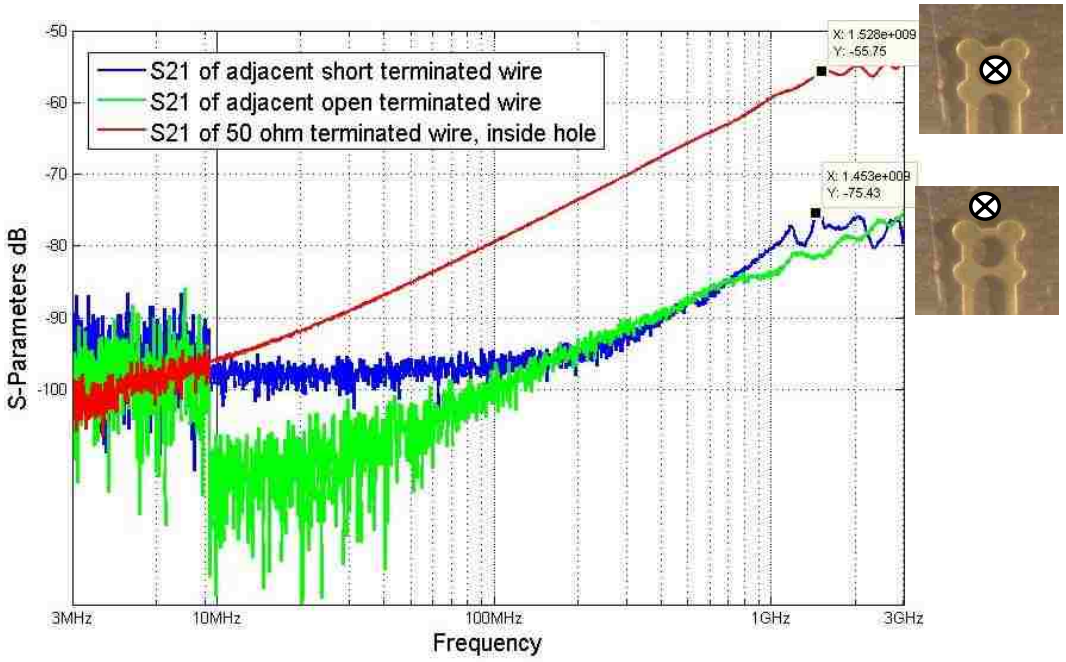

Figure 3.15. Shielding Effectiveness of the BGA Probe

The shielding effectiveness is larger than 20dB above 100MHz, and less than 100MHz, the probe is more sensitive to adjacent current source. Please note that the data

of red line is obtained under 50Ω matched condition. In typical case of measuring a power pin with low impedance, the sensitivity could be 6dB higher.

E-field coupling could be further suppressed by using a hybrid or a differential probe to cancel the common mode components from the output signals.

The internal edges of the slot at probe tip area should be plated, while in this version they are not shielded. In this case, the current version could be only used for measuring outside pins of a BGA probe.

3.1.9. Circuit Modeling and Coupling Mechanisms of the BGA Probe. The equivalent circuit of the whole measurement setup is shown in Figure 3.16; it can be seen as three separate circuits coupled together.

The self-inductance of the excitation wire is guessed as 5nH, which is a reasonable value when considering the wire loop geometry. The inductance would cause non-ideal properties at high frequency region. The ripples of measured S21 around 3GHz could be aroused by such non-idealities.

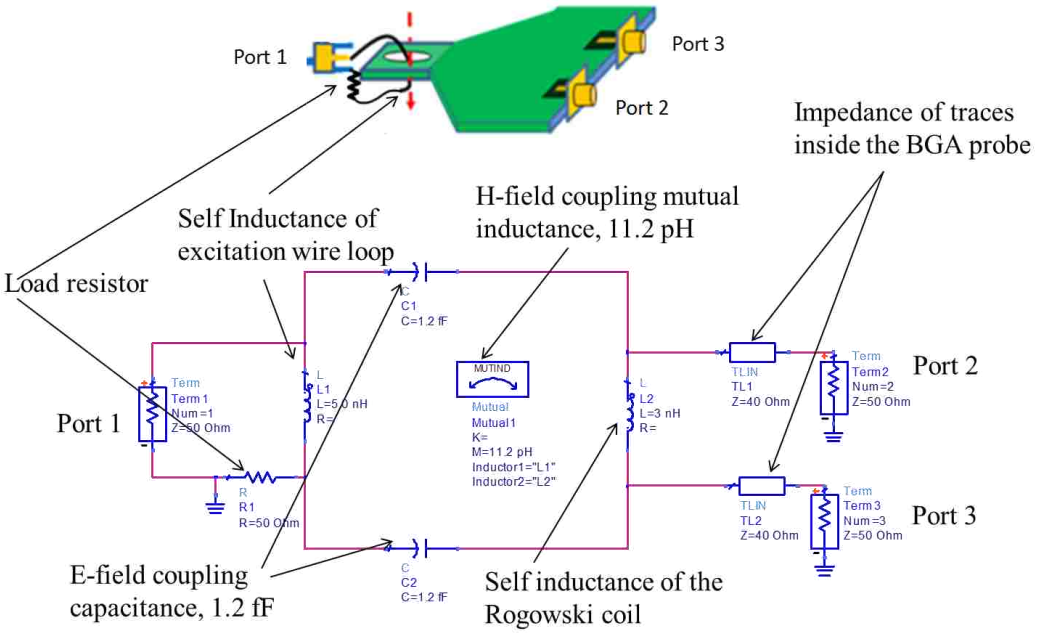

Figure 3.16. Equivalent Circuit of the BGA Probe under Characterization

In the coupling path, mutual capacitance of C1 and C2 stand for the E-field coupling and the mutual inductance Mutual1 represents the H-field coupling path. The mutual inductance is directly related to the Rogowski coil structure that embedded in the probe tip region. Larger cross section area of the Rogowski coil structure or more turns of the coil would lead to higher value of the mutual inductance, and consequently the higher probe sensitivity. And similarly, the larger mutual capacitances are, the higher E-field coupling of the probe suffering.

3.1.9.1 The excitation circuit. The excitation signal is generated from the port 1 of VNA, and the wire which connects the inner & outer conductor of the cable can be considered as an inductor L_W. Apparently, the value of the inductor L_W depends on the size of the loop created by this wire. The current going through the wire is defined as I_Z.

3.1.9.2 The BGA probe. The model of BGA probe includes self-inductance of the Rogowski coil structure, characteristic impedance inside the flex circuit, and port terminations.

3.1.9.3 Coupling path. The coupling path includes mutual inductance, which stands for the H-field coupling, and mutual capacitances, which stands for the E-field coupling, between the BGA probe and excitation circuits.

To obtain the value of mutual inductance, it should be firstly considered that the electromotive force voltage $V_{induced}$ is determined by the current I_z, as

$$j\omega \cdot I_Z \cdot M = V_{induced} \tag{12}$$

where M is the mutual inductance of the Rogowski coil structure.

The Rogowski coil has self-inductance which is noted as L_{self}. When considering the frequency response below a certain frequency, the DUT wire's inductance L_W and the Rogowski coil's self-inductance L_{self} can be ignored. Then, the voltage VNA's port 2, is expressed as:

$$V_{induced} = j\omega \cdot {}^{V_1}/_{R_1} \cdot M \tag{13}$$

$$M = V_{induced} * R_1/(j\omega * V_1) \tag{14}$$

Where R_1 is the source impedance of the VNA's port 1, V_1 is the voltage on port 1. And since

$$S21 = 20 * \log_{10}\left(\frac{V_{induced}}{V_1}\right) \tag{15}$$

Then there is

$$|M| = 10^{\frac{S21}{20}} * \frac{R_S}{\omega} \tag{16}$$

Therefore, if selecting a frequency point with the 20 dB/decade region of the frequency domain response under short condition, the mutual inductance can be calculated. For example, in |S21| equals to -77 dB at 100MHz, and the mutual inductance is calculated as 11.2 pH.

The comparison between equivalent circuit simulation and measurements is shown in Figure 3.17..

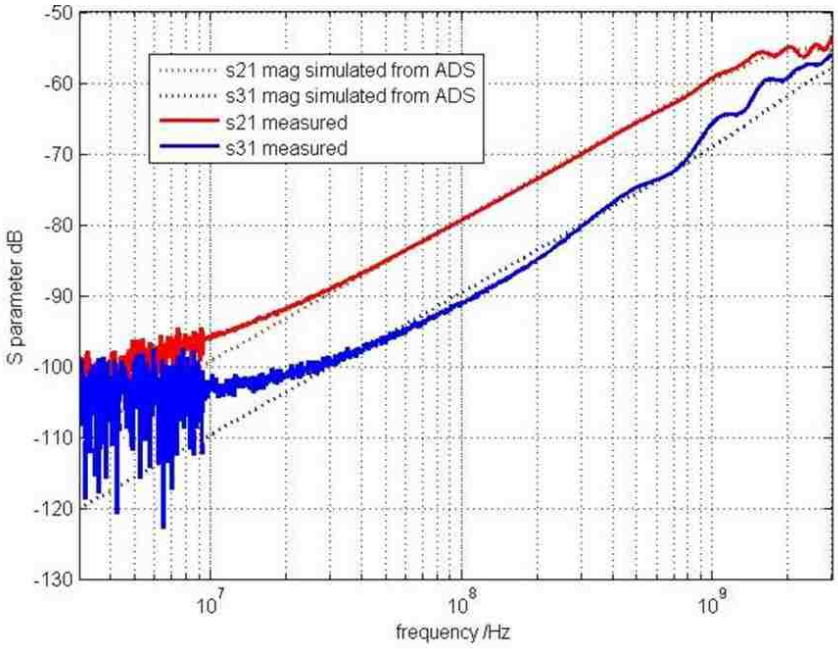

Figure 3.17. Simulation Result of the Equivalent Circuit

ADS simulation results of S21 & S31 shows a 1st order similarity with measured results. This is evidence that the dominant circuit model components such as mutual inductance and capacitance were calculated correctly. In other words, the circuit model showed in last page correctly described the dominant H & E-field coupling mechanism of the BGA probe.

The differences between ADS simulated results and measured result are caused by following factors. Firstly, at low frequency region the probe's sensitivity is so low that H-field coupling is too weak and signals on port 2 and 3 are immersed in noise; secondly, in measurements the geometry of measurement setup is not ideal, therefore the parasitic inductance and capacitance may cause resonances in high frequency range.

3.2. FULL WAVE MODELING AND DESIGN VALIDATION

3.2.1. Introduction of the Full Wave Simulation Model. Before fabrication, the probe was simulated in CST, in order to validate the design. The full wave model of the BGA probe, shown in Figure 3.18 and Figure 3.19, is built similarly to the probe's actual dimensions.

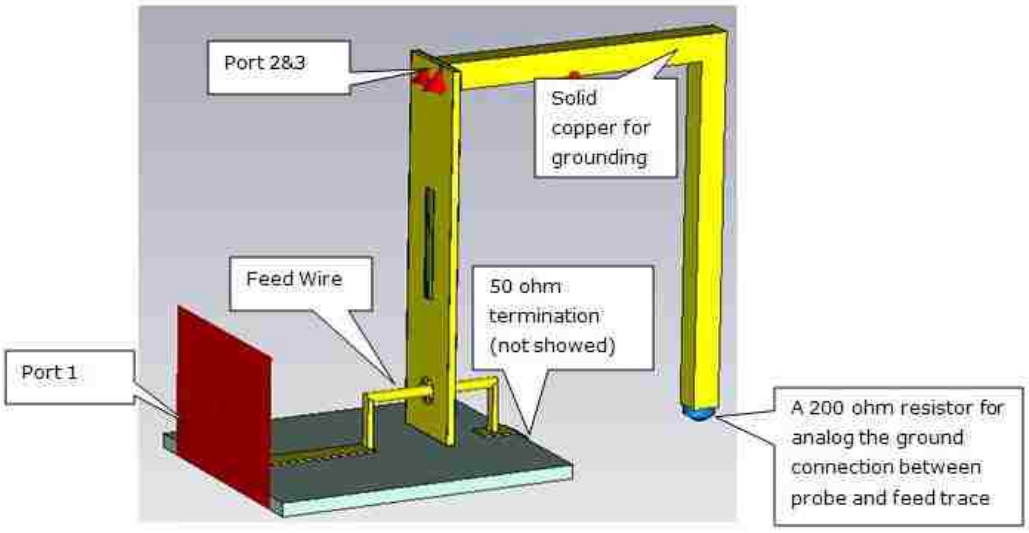

Figure 3.18. Full Wave model of the BGA Probe

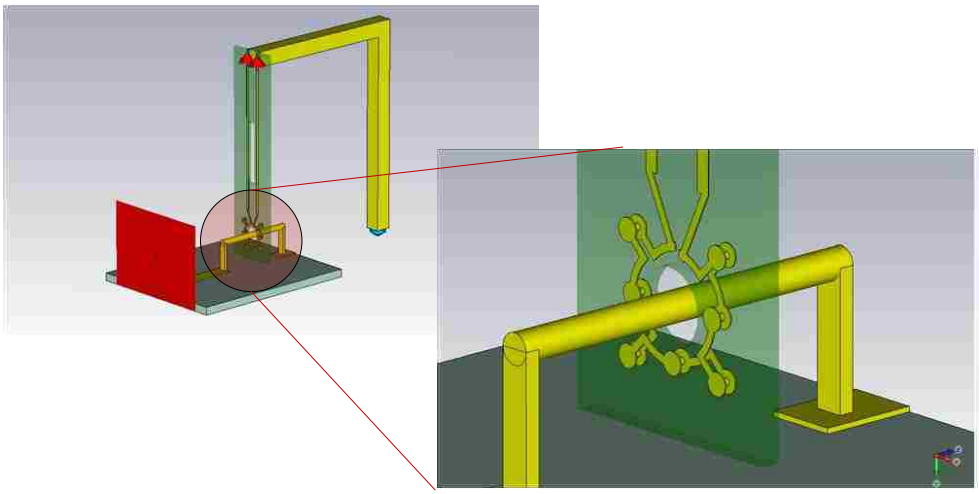

Figure 3.19. Full Wave Model of the BGA Probe, Shielding is Hidden

The full wave model is a simplification of the real-world part, and the apparent structural difference between the simulation model and the real BGA probe is listed as follows:

The model only includes the Rogowski structure, or the tip region of the BGA probe, but not the whole probe assembly. In reality, there are longer microstrip trace on port 2 and 3 inside the flex circuit to route out the signals, and moreover, there are 3 coaxial cables as well as SMA connectors on each port. Since characteristics about the Rogowski Coil structure and critical E-field coupling mechanism are the two factors that only need to be considered in the case, such simplifications are reasonable when building the model.

The feeding wire, or excitation wire, that through the hole should be in curve shape. But in the model, only cylinder and cubic solids used. The measure shouldn't affect the simulation results too much since the coil structure only sensing a very narrow portion of the wire. And this simplification is necessary because simulation time could be reduced significantly, due to much simplified meshing.

The actual probe tip has curled shape but in the model it is in cubic shape. This simplification is acceptable since H-field sensitivity is determined by the Rogowski Coil structure and E-field coupling determined by shielding of the probe, none of which are dominated by outline of the probe tip.

Grounding simplification. The probe's ground, or port 2 and port 3's ground, connects to feeding trace's ground or port 1's ground inside network analyzer. While in this model, they are connected by a large loop solid of copper and a 200 ohm resistor.

3.2.2. Mesh for the CST FDTD Solver. The total mesh cells number of the BGA probe model is about 140K, and the mesh grid is shown in Figure 3.20.

Localized mesh on excitation wire setting is used for calculating the geometry in CST. Such a setting increases mesh density around the Rogowski coil structure, and would generate more precise result.

Before meshing, it is better to optimize curvatures in the geometry to lines. According to experiments, the simulation time would be reduced significantly by using a copper cylinder as the excitation wire, instead of using a wire in curve shape.

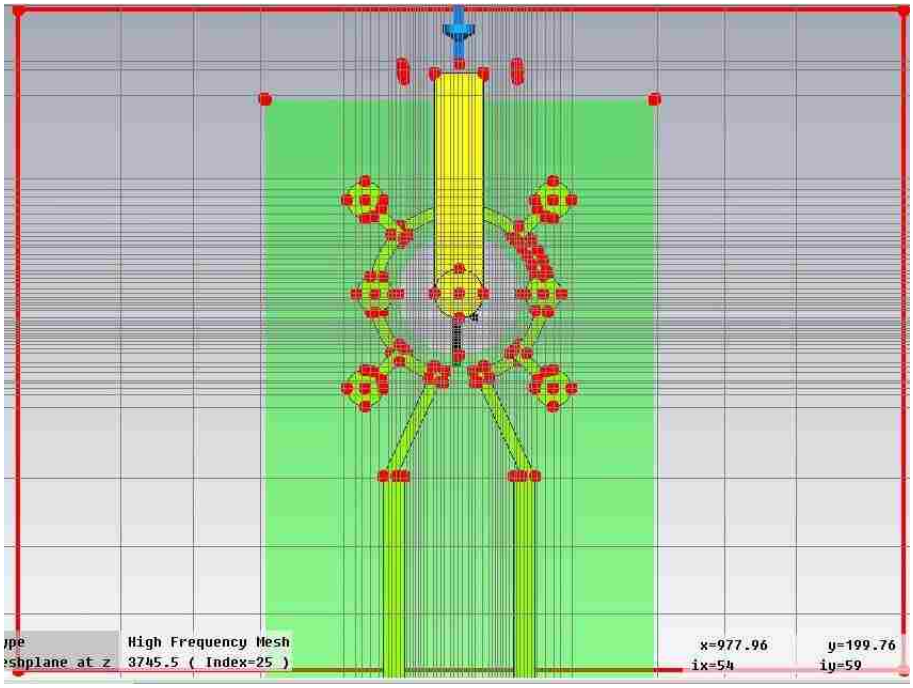

Figure 3.20. Mesh Grid of the BGA Probe Full Wave Model in CST

3.2.3. Full Wave Simulation Result vs. Measurements. Figure 3.21 shows the simulation result, calculated by CST transient solver, and compared against measurement result under 50ohm terminated condition. The measured results conform to simulation results well in the frequency region from 60MHz up to 1.5GHz.

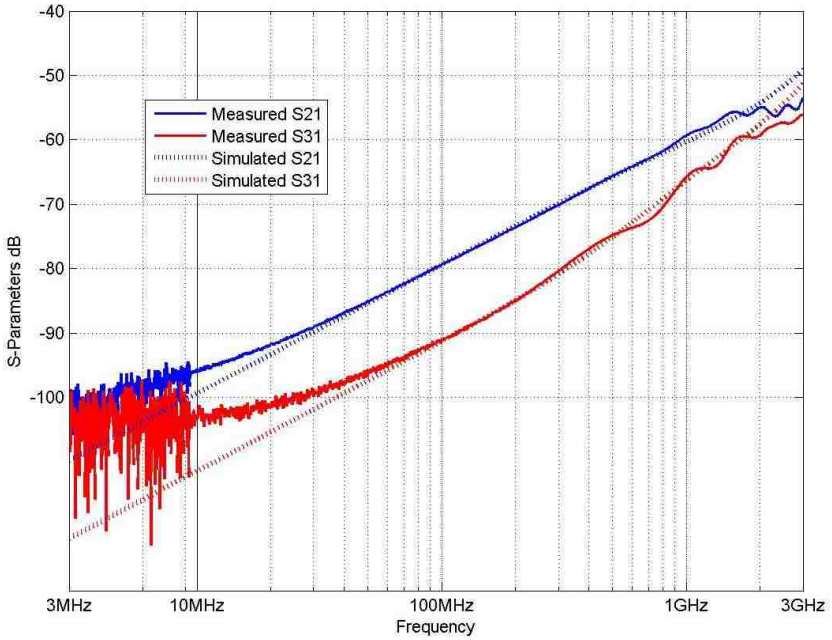

Figure 3.21. Full Wave Simulation vs. Measurements

During experiment, it is found that at higher frequency range, S21 and S31 can be affected much by the feed wire loop geometry. This explains why there's no ripple at the high frequency region of the simulation results, in which case the excitation wire's geometry is more like an ideal case. And at lower frequency range, the measured S21 and S31 have larger values comparing to simulation results, which indicate that the real probe suffers larger common mode and E-field coupling than simulation model. This is because in full wave model, port 2 and 3 are located inside of a shielding case for all directions, which makes simulation is more like an ideal case.

3.3. TIME DOMAIN CHARACTERIZATION

3.3.1. Test Setup for Time Domain Characterization. H-field sensitivity of the BGA probe is not large, so that the probe's output signal in time domain could be rather weak. Amplifiers could be used to solve this issue. A time domain BGA current probing system could be built by connecting the BGA probe assembly together with a differential amplifier and an active oscilloscope probe. The assembly is showed in Figure 3.22.

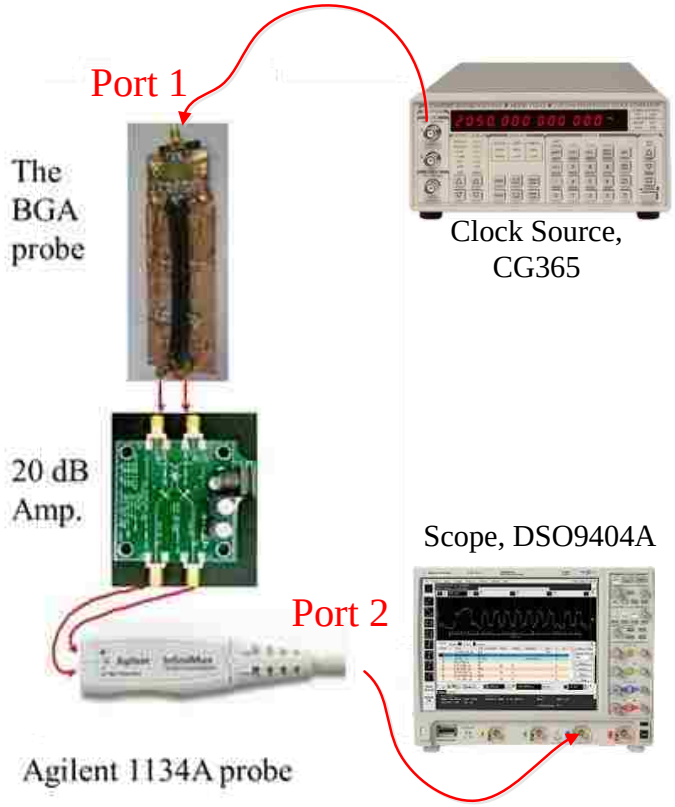

Figure 3.22. BGA Probe with Amplifiers for Time Domain Measurements

Regarding the probing system, time domain excitation current wave, from a 7dBm clock source, is applied to port1. If the frequency response of the probing system is flat, the output time domain signal on port 2 should be similar to the excitation current after calibration; if not, frequency compensation should be applied to correct measured raw data.

3.3.2. Measured Raw Data from Time Domain Measurements. The expected and measured time domain waveforms at port 2 that output from the current probing system, under different clock frequencies, are shown from Figure 3.23 to Figure 3.26. The expected waveforms are shown at the top part of each figure. The measured waveform show same period with the excitation clock, but in different shapes. The phenomena could be explainable since the BGA probe is much less sensitive at low frequency region, which was showed in frequency domain characteristics.

It could be expected that as the frequency of excitation clock increases, the output waveform should be more similar to the input clock

Figure 3.23 shows that the edges of the current-under-test could be constructed well but the steady state cannot, since steady states are low frequency components.

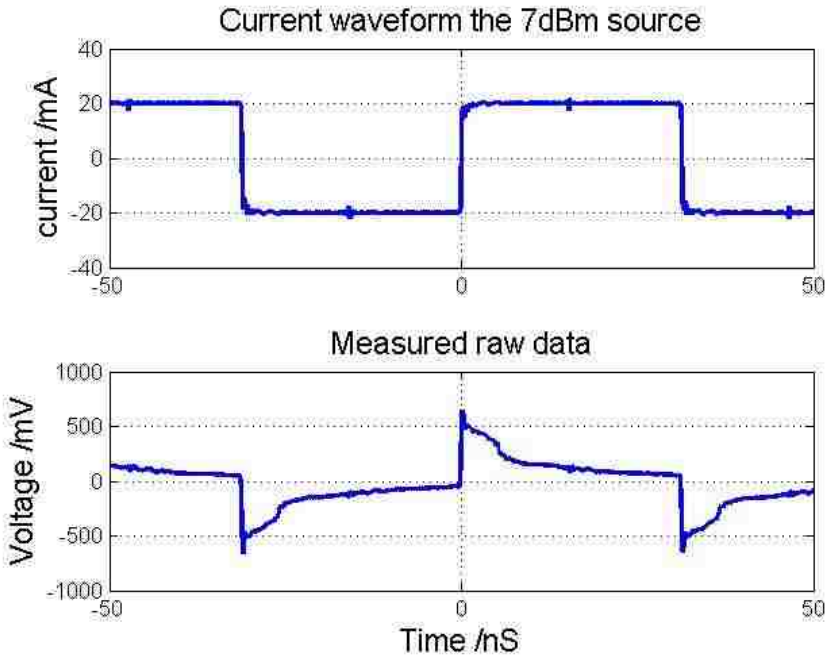

Figure 3.23. Measured Raw Data under 16MHz Clock Excitation

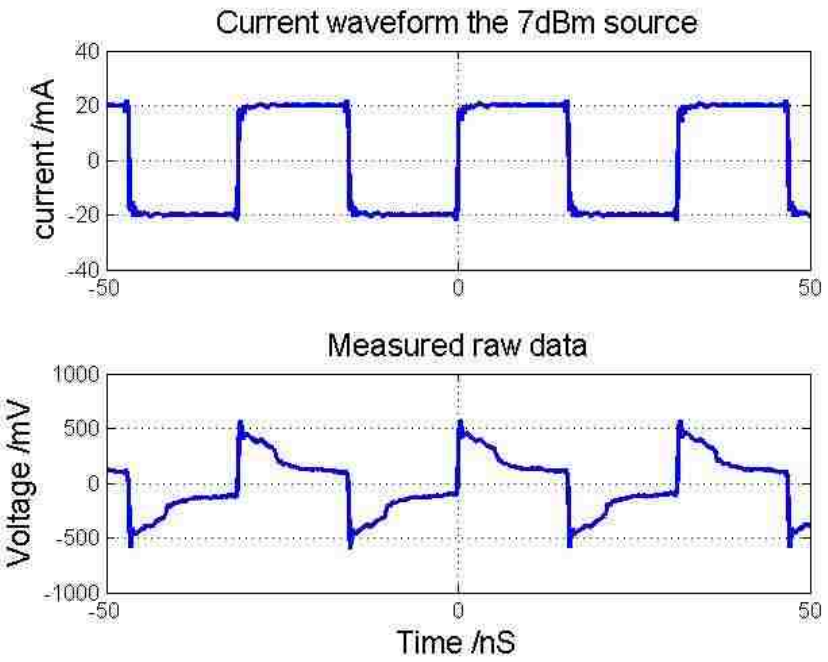

Figure 3.24. Measured Raw Data under 32MHz Clock Excitation

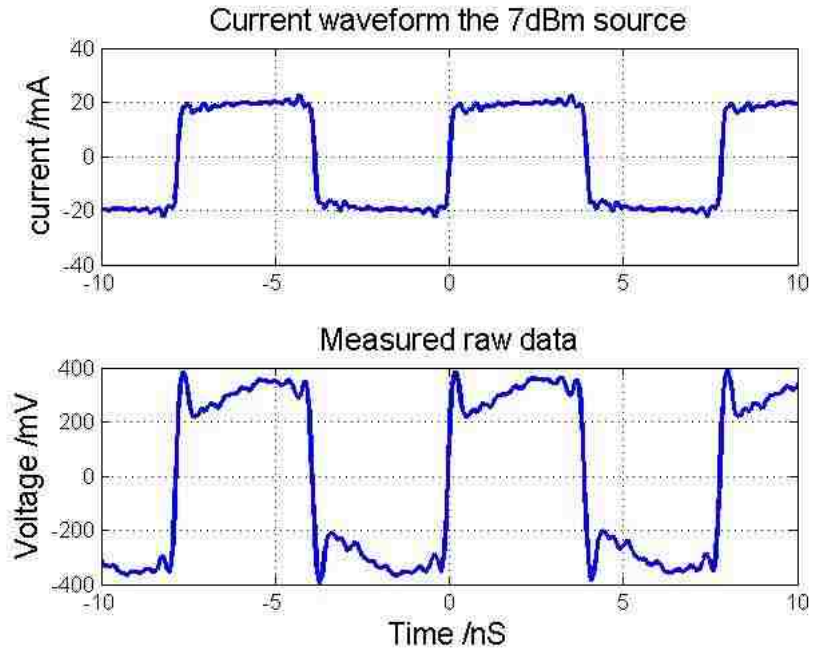

Figure 3.25. Measured Raw Data under 256MHz Clock Excitation

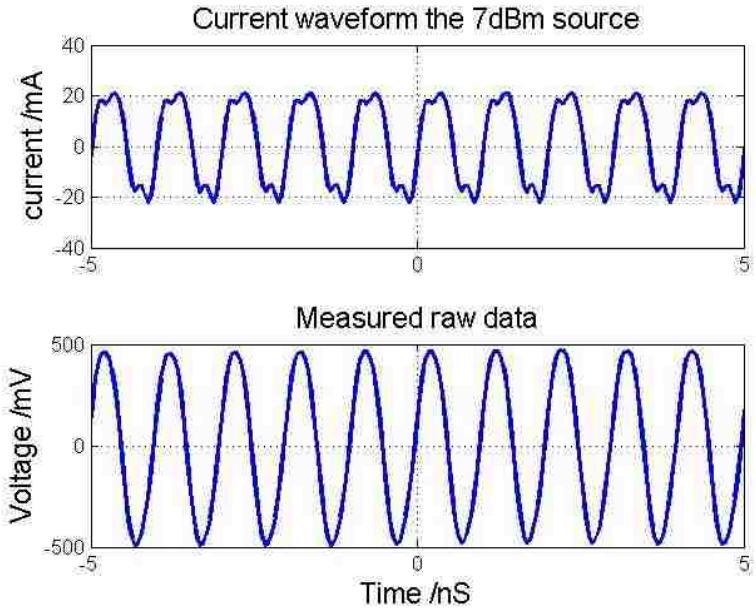

Figure 3.26. Measured Raw Data under 1GHz Clock Excitation

As what shown in the figure, the measured waveform under 256MHz and 1GHz looks more closed to expected waveforms than that of 16MHz and 32MHz cases. Such an observation conforms to the former expectation.

The raw data can be calibrated in order to obtain results that more conforms to expectations. It is necessary to know frequency response of the whole probing system for data correction.

3.3.3. S21 of the Whole Probing System. Measured S21 of the whole probing system is shown in Figure 3.27. The frequency response looks very different with the response of the BGA current probe itself, which was shown in Figure 3.8. This is due to the S21 of the Agilent 1134A active probe.

The 1134A active probe shows a flat response at low frequency, and then goes down as frequency goes higher. This explains why in Figure 3.27, as frequency goes higher, the system S21 shows an increasing trend at low frequency at then start to be flatted around 100MHz. And at high frequencies, the system S21 enters into decreasing region because the BGA probe flat response is flat due to self-integration phenomenon.

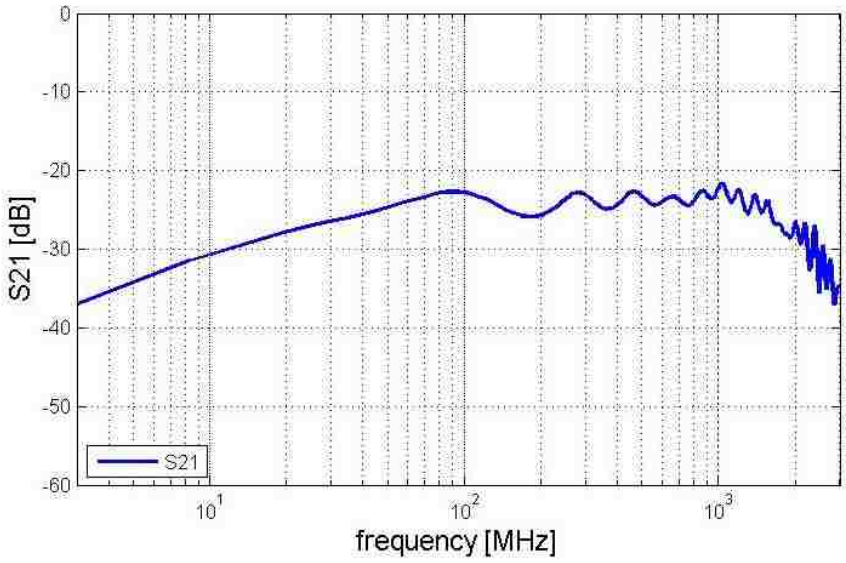

Figure 3.27. S21 of the Whole Probing System

There are two methods to perform frequency domain correction on the measured raw data. One is adding a low frequency compensation network to make the system frequency response more flat; the other method is to programming codes to calibrate measured data mathematically. The first method is more suitable in real time measurements. While the latter one is adopted in this piece of work.

3.3.4. Calibration Algorithm and Programming Scheme. The calibration method is very straight forward. Raw data is transformed into frequency domain and calibrated, then transform back to time domain. The process can be described by the following equation.

$$\mathrm{V_{caliberated}} = ifft[\frac{fft(V_{raw})}{S_{21}}] \tag{17}$$

And after this step, the calibrated result should have similar shape to the actual excitation current waveform, but in the unit of V. Then, the measured current waveform could be calculated by the following equation.

$$\mathrm{I_{measured}} = \frac{V_{caliberated}}{PF} \tag{18}$$

Where PF stands for probe factor, which is in the unit of V/A. The probe factor can be found by comparing the $V_{caliberated}$ with the know excitation current.

The algorithm of data correction could be programmed in Matlab in the process showed in Figure 3.28.

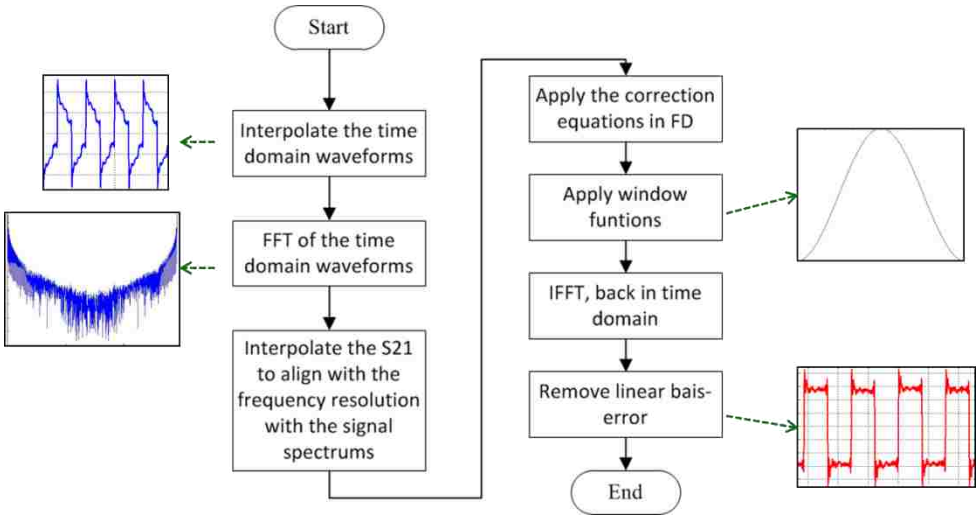

Figure 3.28. The Precedures of the Frequency Domain Data Correction

Before FFT operation, the time domain raw data needs to be interpolated such that its spectrum has the exactly the same length as S21 of the probing system. During calibration, windowing function need to be applied so that the spectrum could decay in high frequency range, in order to avoid high frequency noises after IFFT operation.

3.3.5. Corrected Time Domain Measurement Results. The calibrated results, of that the expiation port of probing system is presented a 7dBm clock with 16MHz, 32MHz, 256MHz and 1GHz, are showed in Figure 3.29 to Figure 3.32.

The calibrated data conforms to the expected current wave, though there with difference of low frequency components, e.g., the expected wave has a flat top while the calibrated data shows a decaying top. This is because that the coil's frequency response decays with 20dB/dec at lower frequencies, thus, that within the dynamic range of the oscilloscope there is less and less useful information at lower frequencies. Consequently,

the needed correction gets stronger the lower the frequency is, leading to large uncertainties, and a strong noise sensitivity towards low frequencies. This shows in the reconstruction of the flat regions of the square wave.

As a conclusion, the probing system is usable for time domain current measurements.

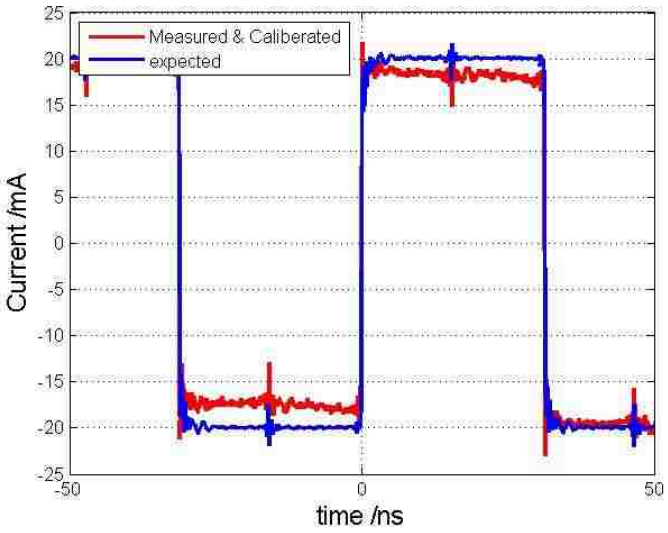

Figure 3.29. Measurement vs. Simulation at 16MHz Clock Excitation

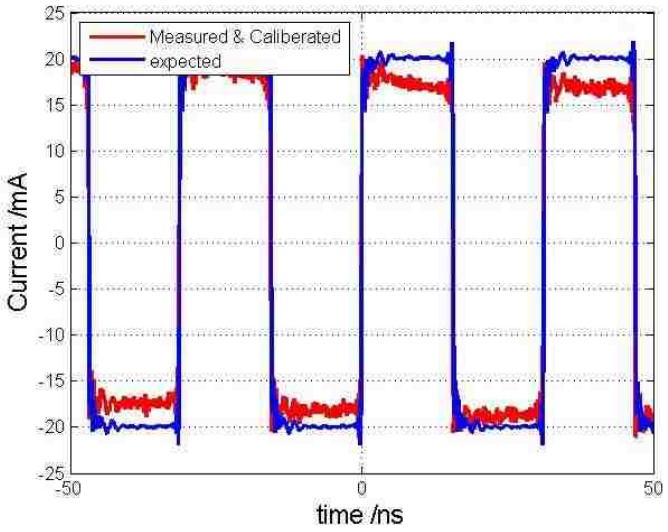

Figure 3.30. Measurement vs. Simulation at 32MHz Clock Excitation

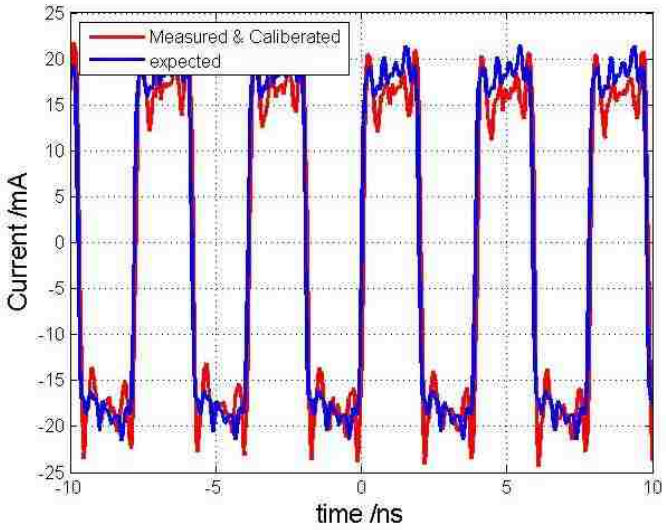

Figure 3.31. Measurement vs. Simulation at 256MHz Clock Excitation

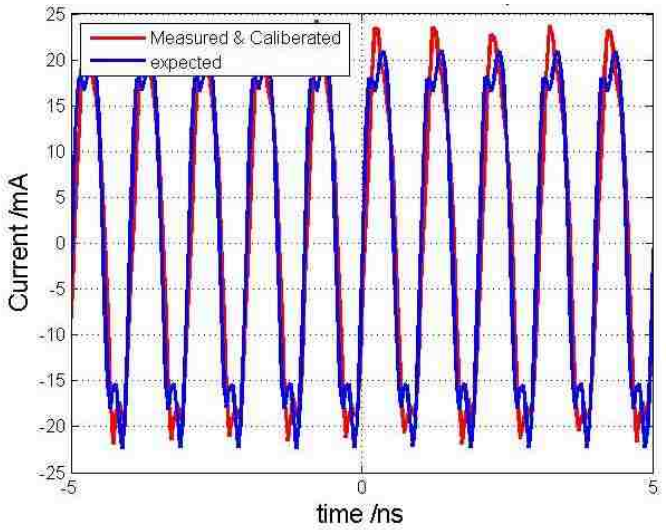

Figure 3.32. Measurement vs. Simulation at 1GHz Clock Excitation

4. A DEMONSTRATION OF USING THE BGA CURRENT PROBE TO MEASURE A BGA-PACKAGED DEVICE

4.1. PLACING BGA CURRENT PROBE UNDER A BGA-PACKAGED DEVICE

Before measurement, the BGA current probe should be placed at the BGA landing area, and in a way that its centered-hole at the probe tip area is aligned with the pad-under-test. Then, the BGA IC is soldered onto the test board. In this way, the test board, the probe and the IC actually constructs like a sandwich.

After measurements, if there's a need to change to another ball to measure, the BGA-packaged IC has to be removed firstly. After re-align the probe to the specified location, re-solder the IC onto the test board and test again.

If there are a lot of needs of changing measurement locations, above measurement process could be troublesome, since the BGA-packaged IC may be damaged after several times of re-soldering works. A BGA socket-adapter pair could solve this problem. It allows users to change the location of the BGA probe, just by plug out the IC, without soldering works. Such kind of configuration is shown in Figure 4.1.

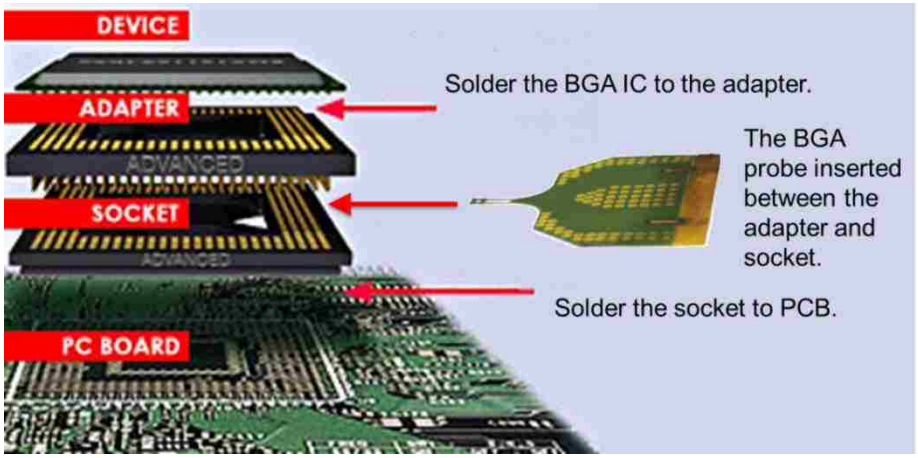

Figure 4.1. The Scheme of Using the BGA Probe with BGA-Adapter-Socket System

In this configuration, the BGA-packaged IC is firstly soldered to an adapter but not the test board. Instead, a socket is soldered to the test board. The BGA current probe could be applied between the adapter and socket, and the probe location can be changed to measure another pin, just by plugging out the IC-adapter out of the socket, instead of re-soldering the IC.

4.2. TEST SETUP FOR MEASURING VDD CURRENTS OF A FPGA DEVICE

A FPGA, Altera's EP1C4F324, is adopted as a DUT that will be measured by the BGA current probe. Accordingly a FPGA test board, showed in Figure 4.2 to Figure 4.4, is designed and manufactured.

Figure 4.2. Top View of the FPGA Test Board

Major parts on the FPGA test board include the FPGA device, configuration circuits, power circuits, a clock source and several output pins. Since there are only a few

peripherals on the board, FPGA's IO current would be very small, and only core current consumption would be tested in this case.

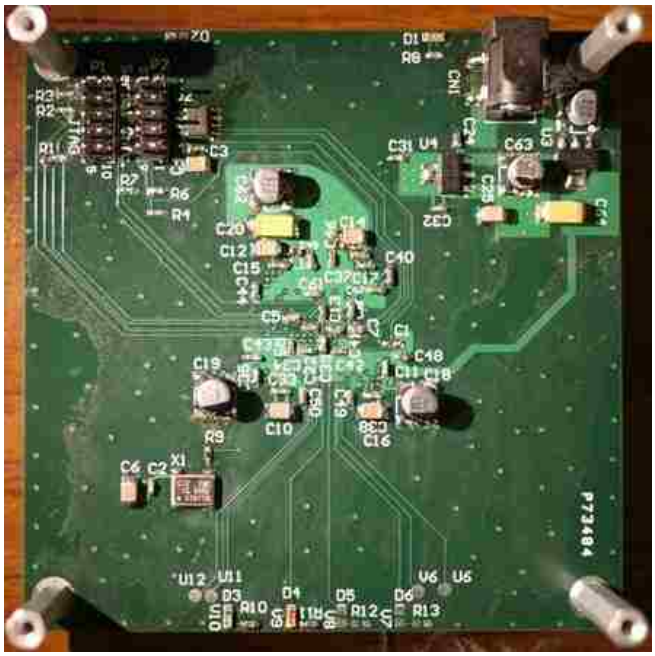

Figure 4.3. Bottom View of the FPGA Test Board

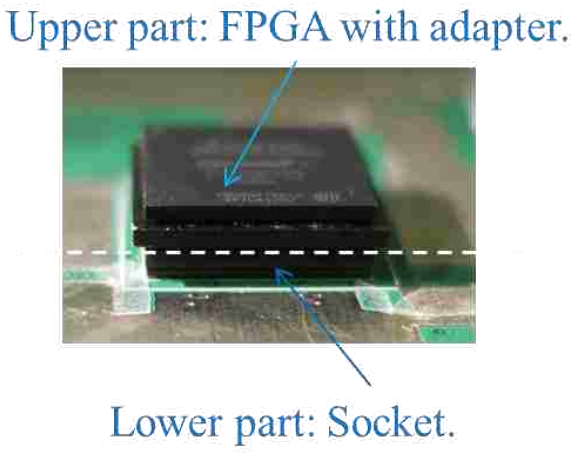

Figure 4.4. Side View of the FPGA Test Board

There is only one component, the FPGA device, on the top side of the FPGA test board.

Configuration circuits, clock source and capacitors and LEDs are mounted at the bottom side of the test board.

The FPGA is programmed to work as a multiplier array. There are 30 groups of multiplier loaded into the FPGA, which take up almost 100% logic resources.

A probe assembly, which is shown in Figure 4.5, is built to measure current of a pin of the FPGA device. There are two coaxial cables, covered with ferrites, are used for routing out the signal.

Figure 4.5. The BGA Current Probe Assembly

During measurements, the probe assembly is placed to the top side of the FPGA test board, in a way such that the center-hole at the probe tip is aligned with the pin-under-test, which is shown in Figure 4.6.

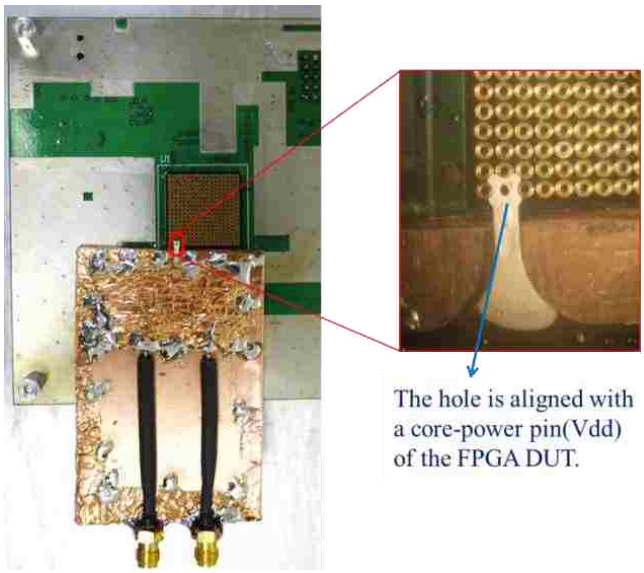

Figure 4.6. Apply the BGA Probe Assembly to the BGA Socket

And then the FPGA IC-Adapter is plugged into the socket. Finished test setup is shown in Figure 4.7.

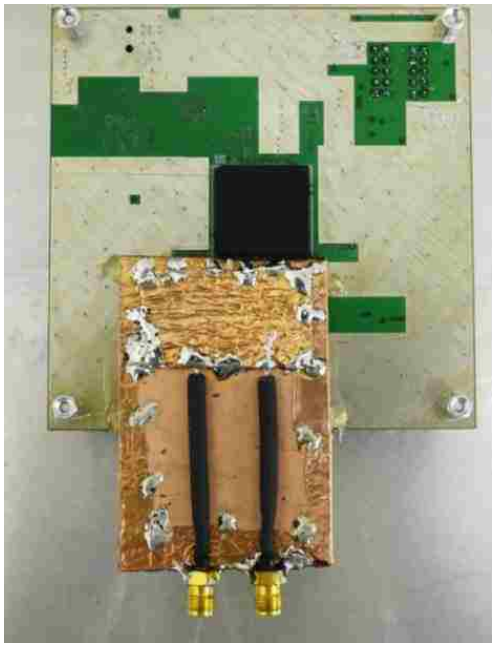

Figure 4.7. The FPGA Test Board with the BGA Probe

Similar to the time domain characterization test, the BGA probe needs to be connected with an amplifier and differential probe. The final test system is shown in Figure 4.8. The oscilloscope Agilent's 1134A is used for measuring.

The whole test setup is placed above a large metal plate, and all exposed grounds of the test board, the amplifier, power supply, and the oscilloscope are connected to the metal plate firmly, in order to reduce the impedance of current return path. This is critical for measuring very weak signals, or otherwise signals will be immersed in common mode noises and cannot be measured.

The amplifier that is inserted between the BGA probe and oscilloscope probe can reduce noise figure of the oscilloscope probe.

The oscilloscope is set to use 50 ohm and AC coupled and 16-average is turned on to reduce the noise. The prerequisite that the average could be used is that the FPGA is programmed in such a way that it behaves exactly the same at each clock cycle.

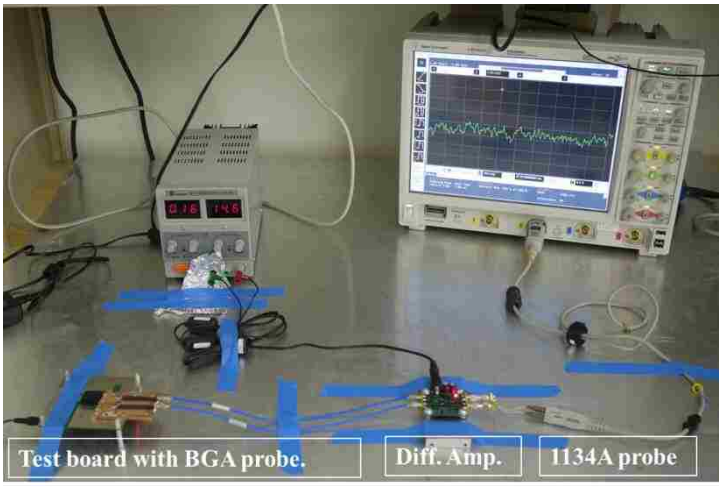

Figure 4.8. The Completed Test Setup for Measuring Currents of a BGA Pin

4.3. MEASURED CURRENT OF A VDD PIN OF THE FPGA DEVICE

The FPGA is loaded with 30 groups of multiplier circuits operating at 16MHz, which take up 98% logic resources of the FPGA device. The inputs of the multipliers are

tied together so that behavior of every multiplier is identical in each clock cycle. The measured current of one Vdd pin, after calibration, is shown in Figure 4.9.

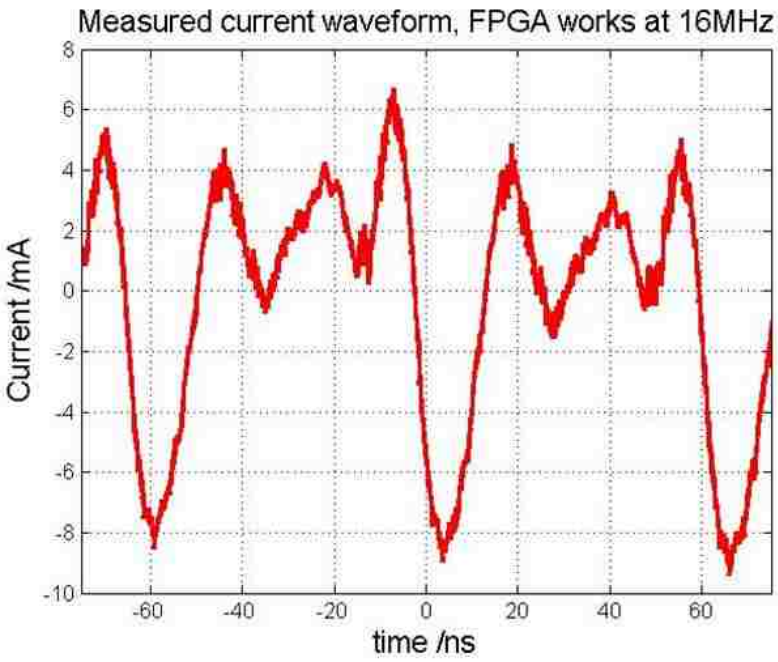

Figure 4.9. Measured Current of the Vdd Pin, FPGA Works at 16MHz Clock, 98% Resources Occupied

It is hard to verify the measured result since there is not a secondary method, till the document is written, to predict the current at a BGA pin.

In this way, the measurement results can only be verified indirectly, i.e., assuming the measured result in Figure 4.9 is correct, then observe if the measured result could conforms to expectations after changing some parameters, like resources occupied, and working frequency.

If changing the operating frequency of the FPGA from 16MHz to a higher frequency, the measured result should show similar waveform but with a shorter period. Such an expectation is validated by measuring the FPGA's current at 24.8MHz, as shown in Figure 4.10

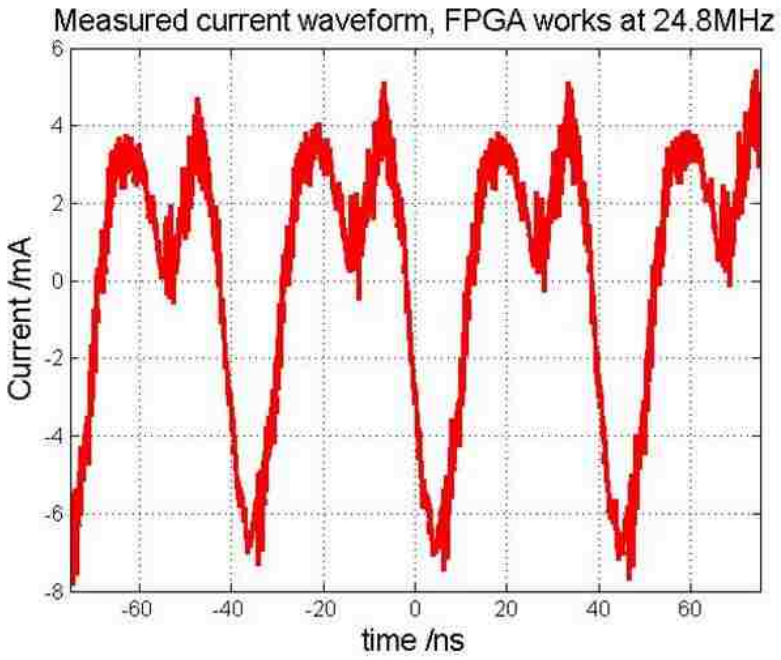

Figure 4.10. Measured Current of the Vdd Pin, FPGA Works at 24.8MHz Clock, 98% Resources Occupied

If keep the clock frequency to 16MHz, and reduce the multiplier groups from 30 to 20, then it could be expected that the measured current waveform should show similar waveform but 1/3 reduction of its amplitude. The measured results conform to such an expectation, as shown Figure 4.11.

The differences between the measured result and expected one might due to that there are several Vdd pins of the FPGA device and the Idd current might not distributed evenly on these Vdd pins.

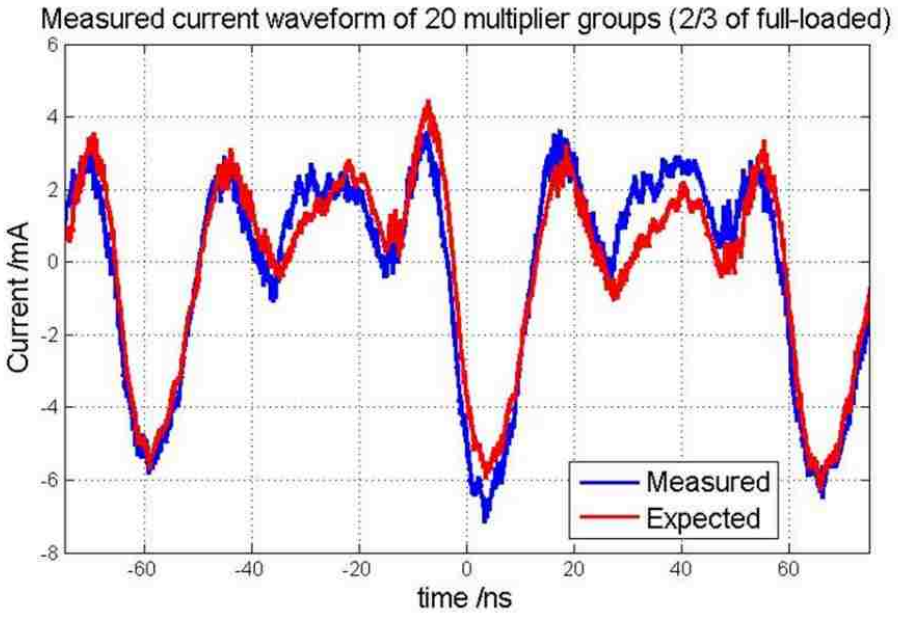

Figure 4.11. Measured Current of the Vdd Pin, FPGA Works at 16MHz Clock, 65% Resources Occupied

5. CONCLUSION

This BGA current probe can be used for measuring currents of a specific ball of a 1mm-BGA devices. And the probe's operating frequency stretches from tens of MHz to GHz.

The probe outputs better results when measuring low-impedance pins, such as a power pin. This is due to the inherent directional coupler property of the BGA current probe. S-parameters, which are shown in Figure 3.12, indicate that

The time domain measurement results on a BGA-packaged FPGA, as shown in Chapter 4, have been to some extent. The result can be fully validated by alternative measurement methods, such as shunt method or using a current clamp to measure the current in an I/O pin. Such a validation would be done later.

The BGA current probe's sensitivity is relatively low so it is necessary to use an amplifier and an active probe to work with the BGA current probe. In this case, the whole probing system needs to be calibrated or to be used in conjunction with a frequency-compensation circuit.

Most of push-to-limit manufacturing challenges, which due to the extremely small feature dimensions, have been solved. Mechanical reliability of the current version is quite good.

In this version, since the long slot at probe tip region is not plated at the internal edges, the probe is only limited to measure outside balls of a BGA package, because E-field coupling might be so strong that screw up measurement results if several balls are placed at in the slot without edge plating.

BIBLIOGRAPHY

[1] I.Zamek, P. Boyle, Z. Li, S. Sun, X. Chen, S. Chandra, T. Li, D. Beetner, and J. Drewniak, "Modeling FPGA Current Waveform and Spectrum and PDN Noise Esteimation," *DesignCon 2008*.

[2] P. R. Palmer, B. H. Stark, J. C. Joyce, "Noninvasive measurement of chip currents in IGBT modules," *Record of IEEE 28th Annual Power Electronics Specialists Conference,* vol. 1, pp. 166 -171, 1997.

[3] C. Xiao, L. Zhao, T. Asada, W. G. Odendaal, J. D. van Wyk, "An Overview of Integratable Current Sensor Technologies," *Conference Record of the 38th IEEE IAS Annual Meeting,* vol. 2, pp. 1251-1258, 12-16 Oct 2003.

[4] J. A. Ferreira, W. A. Cronje, W. A. Relihan, "Integration of high frequency current shunts in power electronic circuits," *IEEE Transactions on Power Electronics,* vol. 10, No. 1, pp. 32 – 37, 1995.

[5] Y. Xu, R. D. Lorenz, "Design of integrated shunt current sensors for IPEMs," *Proc. of CPES Seminar 2002,* pp. 404-411, 2002.

[6] Castelli, F.; , "The flat strap sandwich shunt," *Instrumentation and Measurement, IEEE Transactions* , vol.48, no.5, pp.894-898, Oct 1999

[7] Nassisi, V.; Luches, A.; , "Rogowski coils: theory and experimental results," *Review of Scientific Instruments* , vol.50, no.7, pp.900-902, Jul 1979

[8] D. W. Ackermann, "The Rogowski coil revisited," *Proc. of EPE'01*, Graz, 2001.

[9] Endoh, M.; Shimizu, N.; Yoda, H.; Waoatsuki, N.; , "Highly sensitive thin film magnetoresistive sensor with good linearity," *Electronic Manufacturing Technology Symposium*, 1988, 'Design-to-Manufacturing Transfer Cycle'. *Fifth IEEE/CHMT International* , vol., no., pp.210-214, 10-12 Oct 1988

[10] Morikawa, T.; Nishibe, Y.; Yamadera, H.; Nonomura, Y.; Takeuchi, M.; Taga, Y.; , "Giant magneto-impedance effect in layered thin films," *Magnetics, IEEE Transactions on* , vol.33, no.5, pp.4367-4372, Sep 1997

[11] Iwanami, M.; Hoshino, S.; Kishi, M.; Tsuchiya, M.; , "Magnetic near-field distribution measurements over finite meander circuit patterns by fiber-optic magneto-optic probe," *2003 IEEE International Symposium on Electromagnetic Compatibility*, vol.1, no., pp. 347- 352 vol.1, 18-22 Aug. 2003

[12] Altera Device Package Information, www.altera.com.

VITA

Tianqi Li was born on October 24, 1982, Shannxi Province of P.R.China. He received his Bachelor of Science degree of Communications Engineering in the Electronics Information Engineering Department of Tianjin University, Tianjin, P.R. China.

From March 2004 to June 2009, he worked as a hardware designer at Huawei Technologies Co., Shenzhen, Guangdong Province, P.R. China.

In August 2009, he enrolled at the Missouri University of Science and Technology to pursue his Master's Degree in Electrical Engineering, since when, he was a graduate research assistant in Electromagnetic Compatibility Laboratory. And he received his Master of Science degree in Electrical Engineering in 2011.